SECURITY INFORMATION
CONFIDENTIAL
RESTRICTED

NACA RM L53D08

NACA

RESEARCH MEMORANDUM

LONGITUDINAL STABILITY AND WAKE-FLOW CHARACTERISTICS OF A TWISTED AND CAMBERED WING-FUSELAGE COMBINATION OF 45° SWEEPBACK AND ASPECT RATIO 8 WITH A HORIZONTAL TAIL AND STALL-CONTROL DEVICES AT A REYNOLDS NUMBER OF 4.0×10^6

By Gerald V. Foster

Langley Aeronautical Laboratory
Langley Field, Va.

CLASSIFICATION CHANGED TO UNCLASSIFIED
AUTHORITY: NACA RESEARCH ABSTRACT NO. 99
DATE: APRIL 13, 1956

CLASSIFICATION CHANGED TO
CONFIDENTIAL
BY AUTHORITY J. W. CROWLEY
CHANGE #1628 DATE 12-1-53 T.C.F.

CLASSIFIED DOCUMENT

This material contains information affecting the National Defense of the United States within the meaning of the espionage laws, Title 18, U.S.C., Secs. 793 and 794, the transmission or revelation of which in any manner to an unauthorized person is prohibited by law.

NATIONAL ADVISORY COMMITTEE
FOR AERONAUTICS

WASHINGTON

June 8, 1953

CONFIDENTIAL
RESTRICTED

NATIONAL ADVISORY COMMITTEE FOR AERONAUTICS

RESEARCH MEMORANDUM

LONGITUDINAL STABILITY AND WAKE-FLOW CHARACTERISTICS OF A TWISTED AND CAMBERED WING-FUSELAGE COMBINATION OF 45° SWEEPBACK AND ASPECT RATIO 8 WITH A HORIZONTAL TAIL AND STALL-CONTROL DEVICES AT A REYNOLDS NUMBER OF 4.0×10^6

By Gerald V. Foster

SUMMARY

An investigation has been conducted to determine the effects of a horizontal tail on the longitudinal stability characteristics of a swept-back, twisted and cambered wing in combination with a fuselage and various arrangements of high-lift and stall-control devices. The tests were made at a Reynolds number of 4.0×10^6.

The results indicate that for the tail positions investigated the optimum effect of the horizontal tail on the longitudinal stability of the wing-fuselage combination was obtained with the tail located at 6 percent wing semispan below the wing-root-chord plane. With the tail at this location the minimum change of static margin (0.12 mean aerodynamic chord) through a lift range up to approximately maximum lift coefficient (1.51) was obtained with chord fences located at 57.5 percent and 80.0 percent wing semispan. Some further improvement of the stability characteristics in the range of lift coefficients greater than 1.0 was realized with three or four fences installed on each wing semispan. The leading-edge flaps extending outboard from 52.5 percent wing semispan to approximately the wing tip provided slightly less improvement in the longitudinal stability characteristics than chord fences.

The longitudinal stability of the wing-fuselage combination equipped with a horizontal tail located at the optimum position and either chord fences or leading-edge flaps was adversely affected by extended split flaps deflected 23°.

INTRODUCTION

An extensive investigation has been conducted in the Langley 19-foot pressure tunnel of the low-speed aerodynamic characteristics of a 45° sweptback wing of aspect ratio 8 with and without twist and camber. One wing was twisted and cambered in order to provide an elliptical spanwise loading and a uniform chordwise loading at a lift coefficient of 0.7 and a Mach number of 0.9. The combined effects of twist and camber on the spanwise loading and longitudinal aerodynamic characteristics of the wing are indicated by the results presented in references 1 to 4. References 5 and 6 show the effect of horizontal-tail height on the longitudinal stability characteristics of the wing-fuselage configuration and indicate the advantage to be achieved by the use of the twist and camber and a properly located horizontal tail.

The present paper contains results which extend the information presented in reference 6 concerning the effects of fences on the longitudinal stability of the wing-fuselage-tail combination and includes results obtained with 45-percent-semispan leading-edge flaps and 50-percent-semispan extended split flaps. Results of air-flow surveys made in the region of the horizontal tail are also presented. These data were obtained at a Reynolds number of 4.0×10^6 and a Mach number of 0.19.

SYMBOLS

C_L lift coefficient, $\frac{\text{Lift}}{qS}$

$C_{L_{max}}$ maximum lift coefficient

C_m pitching-moment coefficient about a point $0.0934\bar{c}$ above $0.25\bar{c}$ point of wing, $\frac{\text{Pitching moment}}{qS\bar{c}}$

S wing area, sq ft

S_t tail area, sq ft

$\bar{c}$ mean aerodynamic chord, $\frac{2}{S}\int_0^{b/2} c^2 dy$, ft

c	wing chord, ft
c_t	tail chord, ft
b	wing span, ft
b_t	tail span, ft
y	lateral distance from plane of symmetry
q	free-stream dynamic pressure, $\frac{1}{2}\rho V^2$
ρ	mass density of air
V	free-stream velocity
ϵ	measured local downwash angle, deg
ϵ_e	effective downwash angle, deg (see eq. (2))
q_t/q	ratio of local dynamic pressure at tail to free-stream dynamic pressure
σ	local sidewash angle (inflow negative), deg
α	angle of attack of wing-root chord, deg
$\frac{dC_m}{dC_L}$	rate of change of pitching-moment coefficient with lift coefficient
τ	tail-effectiveness parameter (see eq. (3))
C_{m_t}	pitching-moment coefficient due to tail
$C_{m_{i_t}}$	rate of change of pitching moment with tail incidence angle
$\frac{dC_{m_t}}{d\alpha}$	rate of change of pitching-moment coefficient due to tail with angle of attack
$\left(C_{L_\alpha}\right)_t$	lift-curve slope of isolated tail
α_t	angle of attack of tail, deg (see eq. (1))

l tail length, distance from $0.25\bar{c}$ point of wing to $0.25\bar{c}$ point of tail

i_t incidence angle of horizontal tail measured with respect to wing-root chord, positive when trailing edge is down, deg

i_w angle of incidence of wing with respect to fuselage center line, deg

z vertical distance from wing-root-chord line extended, positive above

δ_f flap deflection, deg

MODEL AND APPARATUS

Figure 1 shows the model mounted on the support struts in the test section of the tunnel. A drawing of the model and some of the geometric characteristics are presented in figure 2. The wing had 45° sweepback along the quarter-chord line, an aspect ratio of 8, a taper ratio of 0.45, and amounts of twist and camber determined by method of reference 7 to provide an elliptical spanwise loading and a uniform chordwise loading at a lift coefficient of 0.7 and a Mach number of 0.9. NACA 63-series airfoil sections having a 12-percent-chord thickness ratio were distributed about a slightly modified $a = 1.0$ mean line (ref. 3) having the desired design lift coefficient. Figure 3 shows the spanwise variation of twist and the distribution of the section design lift coefficient.

The fuselage was circular in cross section and had a fineness ratio of 10. Provisions were made in the fuselage so that the wing could be attached at either 0° or 4° incidence with respect to the fuselage center line.

The horizontal tail had 45° sweepback along the quarter-chord line, an aspect ratio of 4, a taper ratio of 0.45, and NACA 63_1A012 airfoil sections parallel to the plane of symmetry. The tail was mounted on a steel strut which was attached to the fuselage. The vertical height of the tail, defined as the perpendicular distance measured from the wing-root-chord line extended to the $0.25\bar{c}$ of the tail, could be set at various heights ranging from $0.30b/2$ above to $0.15b/2$ below the wing-root chord extended (fig. 2(b)).

Details of fences, leading-edge flaps, and extended split flaps, are shown in figures 2(c), (d), and (e). The fences were made of 1/16-inch sheet steel and were attached perpendicular to the upper

surface of the wing. The fences which extended chordwise from 0.05c or less to the trailing edge are referred to as "chord fences." The fences which extended around the leading edge to 0.25c on the lower surface are referred to as "complete fences." The fence height was varied from 0.10c to 0.018c although throughout the major part of the investigation the fences extended 0.072c above the wing surface. The fences were located on both semispans of the wing at positions indicated in figure 2(c).

The leading-edge flaps extended outboard along the wing leading edge from $0.525b/2$ to $0.975b/2$ (fig. 2(d)).

The extended split flaps had a chord equal to 20 percent of the local wing chord in the undeflected position and could be deflected 23° and 52° from the lower surface of the wing parallel to the plane of symmetry. The flaps extended outboard from the wing-fuselage juncture to $0.50b/2$.

The survey apparatus and the 6-tube rake described in reference 8 were used to measure local values of dynamic pressure, downwash angle, and sidewash angle.

TESTS

The tests were conducted in the Langley 19-foot pressure tunnel with the air compressed to approximately 33 pounds per square inch, absolute. The tests were made at a Reynolds number of 4.0×10^6 and a Mach number of approximately 0.19.

Measurements of lift and pitching moment of the wing-fuselage combination with and without the horizontal tail were made through an angle-of-attack range from -4° to 31°. The various configurations tested are summarized in table I.

Measurements of downwash angle, sidewash angle, and dynamic pressure behind the wing-fuselage configuration $\left(i_w = 4^\circ\right)$ were made in plane normal to the longitudinal axis of the tunnel and $2.93\bar{c}$ behind the quarter chord of the mean aerodynamic chord of the wing. The survey plane represents a compromise between the extreme forward and rearward movement of the quarter-chord point of the mean aerodynamic chord of the tail. The maximum deviation of the $0.25\bar{c}_t$ from the plane of survey occurred at large angles of attack and amounted to 6 percent of the tail length forward of the tail located at $z = -0.06b/2$ and 6 percent tail length rearward for the tail located at $z = 0.30b/2$.

Reduction of Data

The force and moment data have been reduced to nondimensional coefficients and corrected for airstream misalinement, jet-boundary effects, and support tare and interference effects. The jet-boundary corrections were determined by the method of reference 9 and are as follows:

$$\Delta\alpha = 0.39C_L$$

For configuration with tail off,

$$\Delta C_m = 0.0035C_L$$

For configuration with tail on,

$$\Delta C_m = 0.0055C_L$$

All corrections were added.

The air-flow survey data have been corrected for jet-boundary effects by an angle change to the downwash and downward displacement of the flow field. These data are presented in the form of contour charts.

Effective downwash angle.- Values of effective downwash angle were determined from the pitching-moment data obtained with and without the tail. The method by which effective downwash angle was computed is shown by the following equations:

$$\alpha_t = \frac{C_{m_t}}{C_{m_{i_t}}} \tag{1}$$

$$\epsilon_e = \alpha - \alpha_t + i_t \tag{2}$$

where C_{m_t} represents the difference between the pitching-moment coefficient obtained with the tail on and that obtained with the tail off. This procedure of determining effective downwash is based on the premise that the lift of the tail varies linearly with angle of attack of the tail; however, as indicated by results of isolated-tail tests (fig. 4)

this would be true only for a small range of i_t. Since the tail incidence angles were selected to provide a trim condition at moderate and high angles of attack, the tail operated beyond the linear part of the lift curve at low angles of attack of the complete model. Hence the values of effective downwash angle up to approximately 8° angle of attack should be somewhat lower than the values given.

Tail-effectiveness parameter.- The stabilizing contribution of the horizontal tail can be conveniently expressed by a tail-effectiveness parameter τ defined as follows:

$$\tau = -\eta \left[\left(1 - \frac{d\epsilon}{d\alpha} \right) \frac{q_t}{q} + \alpha_t \frac{\partial \frac{q_t}{q}}{\partial \alpha} \right] \tag{3}$$

The values of τ presented herein were obtained by use of the following expression:

$$\tau = \frac{\frac{dC_{m_t}}{d\alpha}}{\frac{S_t}{S} \frac{l}{\bar{c}} \left(C_{l_\alpha} \right)_t} \tag{4}$$

where $\frac{S_t}{S} \frac{l}{\bar{c}} = 0.48$ and $\left(C_{l_\alpha} \right)_t = 0.055$. The tail-efficiency parameter η represents the effective change in the lift-curve slope of the tail due to the effect of fuselage interference. Negative values of τ signify that the tail is contributing stability.

The values of τ presented herein were determined from data which in some cases were considerably out of trim. It may be seen from equation (3) that when $\frac{\partial \frac{q_t}{q}}{\partial \alpha}$ is zero, the magnitude of α_t does not affect the values of τ and therefore the values of τ are applicable to any degree of trim or to any center-of-gravity location. When the term $\frac{\partial \frac{q_t}{q}}{\partial \alpha}$ is of finite value, the changes in α_t required to provide trim were of such a magnitude that the product of the change in α_t and $\frac{\partial \frac{q_t}{q}}{\partial \alpha}$ produced only minor effects on the trends indicated by the curves of τ.

It should be pointed out that the values of τ based on a constant value of $\left(C_{L_\alpha}\right)_t$ underestimate the effectiveness of the tail at low angles of attack of the model due to nonlinearity of the tail lift curve.

RESULTS AND DISCUSSION

Presentation of Data

The effects of the horizontal tail on the lift and pitching-moment characteristics of the wing-fuselage configuration with and without various arrangements of high-lift and stall-control devices are indicated by the data presented in figure 5 and table I. The effects of the horizontal tail located at various vertical positions on the static longitudinal stability are indicated in figure 6 by the variations dC_m/dC_L with lift coefficient. Variations of tail-effectiveness parameter τ with angle of attack are presented in figure 7. Inasmuch as τ is mainly influenced by $d\epsilon_e/d\alpha$, variations of effective downwash angle with angle of attack are also presented in figure 7. The results of air-flow surveys are presented in figures 8 and 9 as contour charts of downwash angle, sidewash angle, and dynamic-pressure ratio. The lack of data at one spanwise station for an angle of attack of 23° necessitated interpolating from a cross plot of the data obtained at a given vertical position relative to the wing-root-chord plane against spanwise position. Shading has been used to designate the contours influenced by interpolated values.

Longitudinal Stability

In general, the longitudinal stability of the plain-wing—fuselage configuration in combination with a horizontal tail was unsatisfactory. The variations of dC_m/dC_L (figs. 6(a) and (b)) indicate that, although the tail at all vertical positions investigated improved the stability, dC_m/dC_L became positive above a lift coefficient of 0.7 as in the case of the tail-off configuration. Reference 4 indicates that the instability at moderate and high lift coefficients, due primarily to a loss in lift effectiveness of the outboard sections of the wing, can be substantially improved through the use of fences to control the boundary-layer cross flow. A comparison of the results presented in figures 6(c) and (d) with those in figure 6(a) indicates that fences markedly improved the stability of the tail-on and tail-off configurations through the moderate and high lift-coefficient range. It may also be noted that because of the improvement provided by the fences the differences in effectiveness of the horizontal tail at various vertical locations become more significant. The

variations of dC_m/dC_L for the configuration equipped with chord fences located at 0.575b/2 and 0.80b/2 and the horizontal tail located at z = -0.06b/2 indicate that the change in the static margin through a lift range up to almost $C_{L_{max}}$ (1.51) was relatively small and amounted to approximately 0.12 mean aerodynamic chord; whereas, with the horizontal tail located at z = 0.14b/2, the change in static margin was approximately 0.22 mean aerodynamic chord.

Reference 4 indicates that more than two fences provided a greater improvement in the stability characteristics of the wing alone prior to $C_{L_{max}}$ than with two fences. The variation of dC_m/dC_L with C_L (fig. 6(d)) indicates that with four fences installed on the airplane configuration the stability was markedly increased through a range of lift coefficients from approximately 1.0 up to almost $C_{L_{max}}$ with the tail located at either z = 0.14b/2 or -0.06b/2. A similar change in the stability was also noted with three complete fences located at 0.45b/2, 0.70b/2, and 0.89b/2 (table I). Considering the effects of various fence configurations on the longitudinal stability characteristics, the minimum change in the static margin through the lift range was obtained with fences located at 0.575b/2 and 0.80b/2.

A comparison of the curves of dC_m/dC_L presented in figures 6(c), (d), and (g) indicates that the improvement in the stability characteristics of the tail-on configuration was slightly greater with either multifence arrangement than with 0.45b/2 leading-edge flaps. The difference in stability of the tail-on configuration equipped with fences or leading-edge flaps is associated primarily with the difference in effectiveness of these devices on the stability characteristics of tail-off configuration.

The addition of 0.50b/2 extended split flaps ($\delta_f = 23°$) had an adverse effect on the stability characteristics obtained with the horizontal tail at all vertical positions investigated. With the tail located at z = -0.06b/2 and the wing equipped with either chord fences located at 0.575b/2 and 0.80b/2 or with 0.45b/2 leading-edge flaps, the addition of 0.50b/2 extended split flaps produced an additional increase of approximately 0.13 mean aerodynamic chord in the change of static margin through the lift range up to approximately $C_{L_{max}}$ (see figs. 6(c), (e), (g), and (i)).

It is interesting to note that, with the horizontal tail located at z = 0.14b/2, the addition of the extended split flaps ($\delta_f = 23°$) produced a change of the static margin through a lift range up to approximately $C_{L_{max}}$ which was appreciably larger with the wing equipped with leading-edge flaps than with chord fences (figs. 6(e) and (i)). The large change

of static margin of the wing-fuselage combination equipped with 0.45b/2 leading-edge flaps and 0.50b/2 extended split flaps ($\delta_f = 23^\circ$) was markedly reduced when the angle of deflection of the split flaps was increased from 23° to 52° or by the addition of chord fences located at 0.575b/2 and 0.80b/2 (figs. 6(i), (j), and (h)). The improvement in the stability characteristics with chord fences resulted essentially from an improvement in the stability characteristics of the tail-off configuration just prior to $C_{L_{max}}$; whereas, increasing the angle of deflection of the split flaps in combination with leading-edge flaps tended to increase the effectiveness of the horizontal tail located at $z = -0.06b/2$ and 0.14b/2. The change of static margin through the lift-coefficient range from approximately 0.2 up to approximately $C_{L_{max}}$ of the configuration with the horizontal tail located at $z = -0.06b/2$, 0.45b/2 leading-edge flaps, and extended split flaps deflected 52° was approximately 0.14 mean aerodynamic chord.

Horizontal-Tail Effectiveness

The effectiveness of the tail varied with its vertical position in a manner similar to that indicated by previous investigations of a swept-wing airplane configuration with tail lengths ranging from 1.7 to 3.0 (for example, see refs. 5 and 10). The values of τ for the flap-neutral configuration, fences off, (fig. 7(b)) indicate that at moderate and high angles of attack the tail located 0.14b/2 above the wing-root-chord line extended was more effective than the tail located 0.30b/2 above the wing-root-chord line extended. This difference in tail effectiveness results primarily from a more favorable variation of downwash angle with angle of attack below the wake center than above the wake center. It may be noted from the contours of dynamic-pressure ratio that the tail located at $z = 0.14b/2$ has moved down to approximately the center of the wake at an angle of attack of 19° (fig. 8(c)); whereas, the tail located at $z = 0.30b/2$ is still approximately 0.10b/2 above the center of the wake at an angle of attack as high as 25° (fig. 8(d)).

A comparison of the values of τ presented in figures 7(e) to (i) with those shown in figures 7(a) and (b) indicates that addition of the extended split flaps in combination with stall-control devices tended to alter the effectiveness of the tail. A comparison of the contours of dynamic-pressure ratio (figs. 8 and 9) indicates that an appreciable shift in the wake center resulted with the extended split flaps deflected 23° and fences. The influence of the split flaps on the wake resulted in changes of τ which occurred at low angles of attack for the tail located at $z = 0.06b/2$ and at high angles of attack for the tail located at $z = 0.30b/2$. It is believed that the split flaps caused the major part of the change in the tail effectiveness since the addition of either type of stall-control device without the split flap present had

a negligible influence on the effectiveness of the tail located either above or below the wing-root-chord line extended.

CONCLUDING REMARKS

The results of an investigation of the low-speed longitudinal stability characteristics of a twisted and cambered wing having sweepback of 45° and an aspect ratio of 8 in combination with a fuselage and a horizontal tail indicate that:

For the tail positions investigated, the optimum effect of the horizontal tail on the longitudinal stability of the wing-fuselage combination was obtained with the tail located at 6 percent wing semispan below the wing-root-chord plane. With the tail located at this position the minimum change of static margin (0.12 mean aerodynamic chord) through a lift range up to approximately maximum lift coefficient (1.51) was obtained with chord fences located at 57.5 percent and 80.0 percent wing semispan. Some further improvement of the stability characteristics in the range of lift coefficients greater than 1.0 was realized with three or four fences installed on each wing semispan. The leading-edge flaps extending outboard from 52.5 percent wing semispan to approximately the wing tip provided slightly less improvement in the longitudinal stability characteristics than chord fences.

The longitudinal stability of the wing-fuselage combination equipped with a horizontal tail located at the optimum position and either chord fences or leading-edge flaps was adversely affected by extended split flaps deflected 23°.

Langley Aeronautical Laboratory,
National Advisory Committee for Aeronautics,
Langley Field, Va.

REFERENCES

1. Graham, Robert R.: Low-Speed Characteristics of a 45° Sweptback Wing of Aspect Ratio 8 From Pressure Distributions and Force Tests at Reynolds Numbers From 1,500,000 to 4,800,000. NACA RM L51H13, 1951.

2. Pratt, George L., and Shields, E. Rousseau: Low-Speed Longitudinal Characteristics of a 45° Sweptback Wing of Aspect Ratio 8 With High-Lift and Stall-Control Devices at Reynolds Numbers From 1,500,000 to 4,800,000. NACA RM L51J04, 1952.

3. Pratt, George L.: Effects of Twist and Camber on the Low-Speed Longitudinal Stability Characteristics of a 45° Sweptback Wing of Aspect Ratio 8 at Reynolds Numbers From 1.5×10^6 to 4.8×10^6 as Determined by Pressure Distributions, Force Tests, and Calculations. NACA RM L52J03a, 1952.

4. Salmi, Reino J.: Low-Speed Longitudinal Aerodynamic Characteristics of a Twisted and Cambered Wing of 45° Sweepback and Aspect Ratio 8 With and Without High-Lift and Stall-Control Devices and a Fuselage at Reynolds Numbers From 1.5×10^6 to 4.8×10^6. NACA RM L52C11, 1952.

5. Salmi, Reino J., and Jacques, William A.: Effect of Vertical Location of Horizontal Tail on the Static Longitudinal Stability Characteristics of a 45° Sweptback-Wing - Fuselage Combination of Aspect Ratio 8 at a Reynolds Number of 4.0×10^6. NACA RM L51J08, 1952.

6. Foster, Gerald V.: Effects of Twist and Camber, Fences, and Horizontal-Tail Height on the Low-Speed Longitudinal Stability Characteristics of a Wing-Fuselage Combination With a 45° Sweptback Wing of Aspect Ratio 8 at a Reynolds Number of 4.0×10^6. NACA RM L52J03, 1952.

7. Cohen, Doris: A Method for Determining the Camber and Twist of a Surface To Support a Given Distribution of Lift, With Applications to the Load Over a Sweptback Wing. NACA Rep. 826, 1945. (Supersedes NACA TN 855.)

8. Furlong, G. Chester, and Bollech, Thomas V.: Downwash, Sidewash, and Wake Surveys Behind a 42° Sweptback Wing at a Reynolds Number of 6.8×10^6 With and Without a Simulated Ground. NACA RM L8G22, 1948.

9. Sivells, James C., and Salmi, Rachel M.: Jet-Boundary Corrections for Complete and Semispan Swept Wings in Closed Circular Wind Tunnels. NACA TN 2454, 1951.

10. Griner, Roland, F., and Foster, Gerald V.: Low-Speed Longitudinal and Wake Air-Flow Characteristics at a Reynolds Number of 6.0×10^6 of a 52° Sweptback Wing Equipped With Various Spans of Leading-Edge and Trailing-Edge Flaps, a Fuselage, and a Horizontal Tail at Various Vertical Positions. NACA RM L50K29, 1951.

TABLE I

SUMMARY OF PITCHING-MOMENT CHARACTERISTICS OF AN AIRPLANE MODEL HAVING A 45° SWEPTBACK, TWISTED AND CAMBERED WING

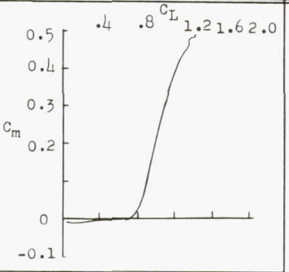
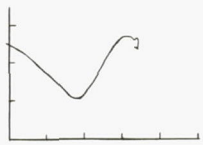
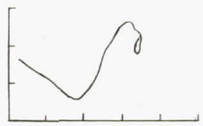
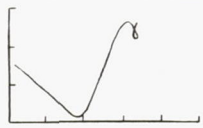
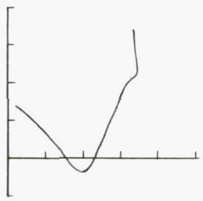
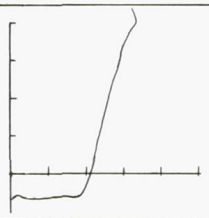
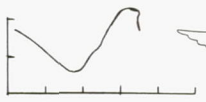
Span of L.E. device, b/2	Span of T.E. device, b/2	Fence location, b/2	Tail height, percent wing semispan from wing-root chord extended	C_m Characteristics	Figure
None	None	None	Tail off; $i_w = 0°$		5(a)
			-15; $i_w = 0°$		
			4.5; $i_w = 0°$		
			14.0; $i_w = 0°$		
			30.0; $i_w = 0°$		
			Tail off; $i_w = 4°$		
			-6.0; $i_w = 4°$		

TABLE I.- Continued

SUMMARY OF PITCHING-MOMENT CHARACTERISTICS OF AN AIRPLANE MODEL HAVING A 45° SWEPTBACK, TWISTED AND CAMBERED WING

Span of L.E. device, b/2	Span of T.E. device, b/2	Fence location, b/2	Tail height, percent wing semispan from wing-root chord extended	C_m Characteristics	Figure
None	None	Fence height 0.072c; .575; .80	Tail off; $i_w = 4°$	C_m vs C_L (0.3, 0.2, 0.1, 0; -0.1; .4, .8, 1.2, 1.6, 2.0)	5(b)
			-6.0; $i_w = 4°$		
			14.0; $i_w = 4°$		
			30.0; $i_w = 4°$		
		Fence height 0.018c 0.072c; .575; .80	Tail off; $i_w = 4°$		--
			-6.0; $i_w = 4°$		
		Fence height 0.072c; .45; .70; .89	Tail off; $i_w = 4°$		
			-6.0; $i_w = 4°$		
		Fence height 0.072c; .35; .575; .80; .89	Tail off; $i_w = 4°$		5(c)

NACA

TABLE I.- Continued

SUMMARY OF PITCHING-MOMENT CHARACTERISTICS OF AN AIRPLANE MODEL HAVING A 45° SWEPTBACK, TWISTED AND CAMBERED WING

Span of L.E. device, b/2	Span of T.E. device, b/2	Fence location, b/2	Tail height, percent wing semispan from wing-root chord extended.	C_m Characteristics	Figure
None	None	.35, .575, .80, .89; Fence height 0.072c	-6.0; $i_w = 4°$	C_m vs C_L: 0.2, 0.1, 0, -0.1; .4 .8 C_L 1.2 1.6 2.0	5(c)
			14.0; $i_w = 4°$		
			30.0; $i_w = 4°$		
.45L.E. flap	None	None	Tail off; $i_w = 4°$		5(d)
			-6.0; $i_w = 4°$		
			$i_w = 4°$; 14.0		
			$i_w = 4°$; 30.0		
None	.5 ext split flap $\delta_f = 23°$	.575, .80; Fence height 0.072c	Tail off; $i_w = 4°$		5(e)
			-6.0; $i_w = 4°$		

TABLE I.- Continued

SUMMARY OF PITCHING-MOMENT CHARACTERISTICS OF AN AIRPLANE MODEL HAVING A 45° SWEPTBACK, TWISTED AND CAMBERED WING

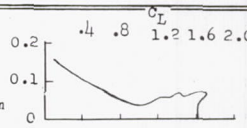
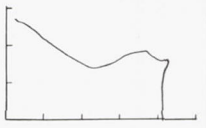
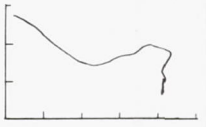
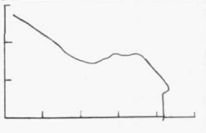
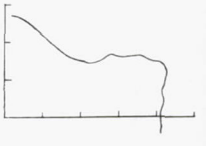
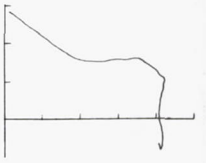
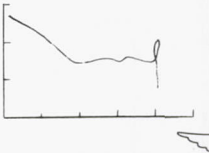
Span of L.E. device, b/2	Span of T.E. device, b/2	Fence location, b/2	Tail height, percent wing semispan from wing-root chord extended	C_m Characteristics	Figure
None	.5 ext split flaps δ_f=23°	Fence height 0.072c at .575 to .80	14.0; i_w = 4°		5(e)
		Fence height 0.072c at .625 to .80	-6.0; i_w = 4°		--
		Fence height 0.072c at .70 to .80	-6.0; i_w = 4°		
		Fence height 0.10c at .70 to .80	-6.0; i_w = 4°		
		Fence height 0.072c at .525 to .80	-6.0; i_w = 4°		
		Fence height 0.072c at .625 to .80	-6.0; i_w = 4°		
		Fence height 0.072c at .575 to .70	-6.0; i_w = 4°		
		Fence height 0.072c at .575 to .80	-6.0; i_w = 4°		

TABLE I.- Continued

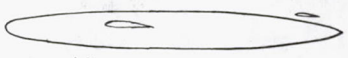
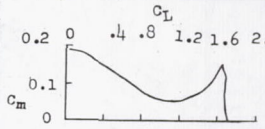
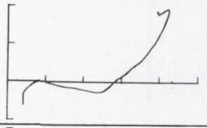
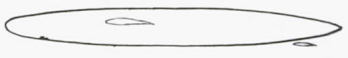
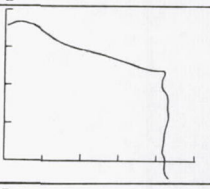
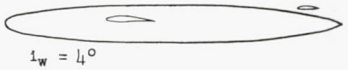
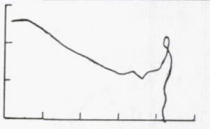
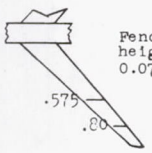
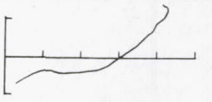
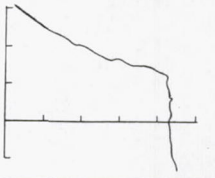
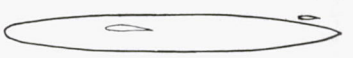
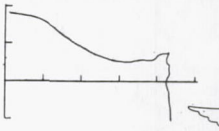
SUMMARY OF PITCHING-MOMENT CHARACTERISTICS OF AN AIRPLANE

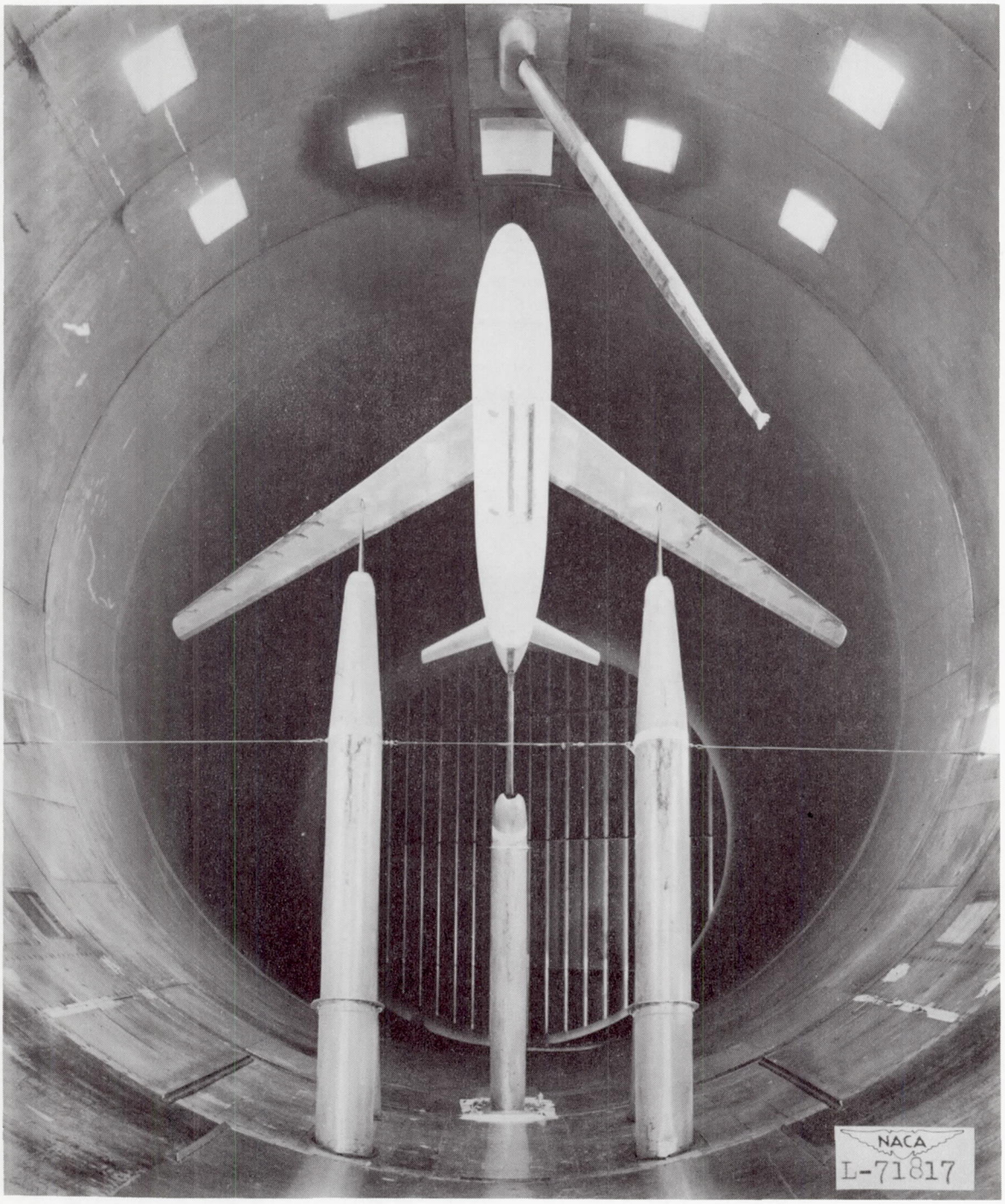
MODEL HAVING A 45° SWEPTBACK, TWISTED AND CAMBERED WING

Span of L.E. device, b/2	Span of T.E. device, b/2	Fence location, b/2	Tail height, percent wing semispan from wing-root chord extended	C_m Characteristics	Figure
None	.5 ext. split flap $\delta_f=23°$	Fence height .575 .036c .80 .072c	-6.0 $i_w = 4°$	C_m vs C_L (0.3, 0.2, 0.1, 0; .4.8 C_L 1.2 1.6 2.0)	--
		Fence height .575 .018c .80 .072c	-6.0 $i_w = 4°$		
		Fence height .575 .018c .80	-6.0 $i_w = 4°$		
		Fence height 0.072c .35 .575 .80 .89	Tail off $i_w = 4°$		5(f)
			-6.0 $i_w = 4°$		
			14.0 $i_w = 4°$		
			$i_w = 4°$ 30.0		
.415L.E. flap	.5 ext. split flap $\delta_f=23°$	None	Tail off $i_w = 4°$		5(g)
			-6.0 $i_w = 4°$		

TABLE I.- Concluded

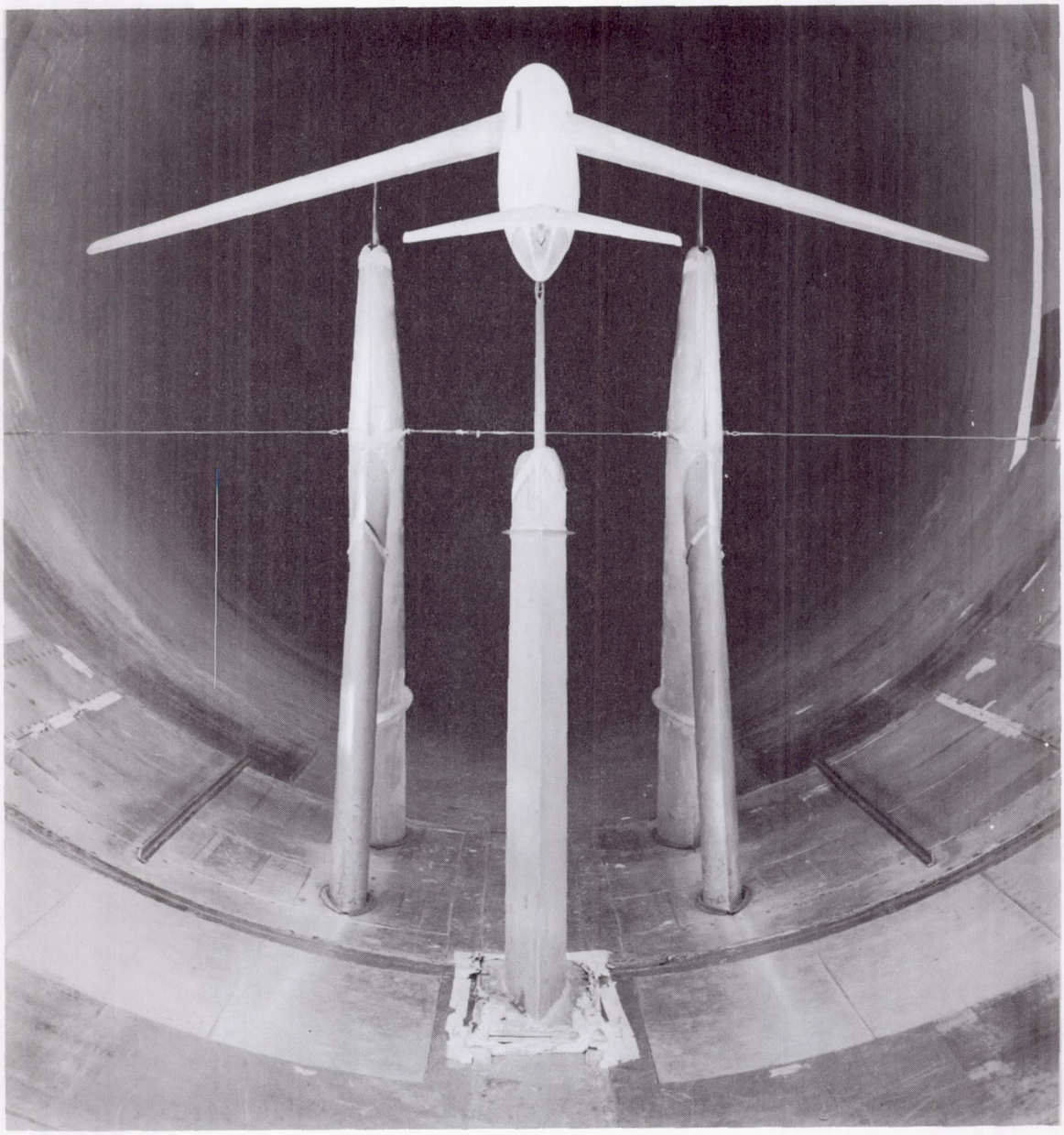
SUMMARY OF PITCHING-MOMENT CHARACTERISTICS OF AN AIRPLANE MODEL HAVING A 45° SWEPTBACK, TWISTED AND CAMBERED WING

Span of L.E. device, b/2	Span of T.E. device, b/2	Fence location, b/2	Tail height, percent wing semispan from wing-root chord extended	C_m Characteristics	Figure
.45 L.E. flap	.5 ext split flap $\delta_f=23°$	None	14.0  $i_w = 4°$		5(g)
	.5 ext split flap $\delta_f=52°$	None	Tail off  $i_w = 4°$		5(h)
			-6.0  $i_w = 4°$		
			14.0  $i_w = 4°$		
	.5 ext. split flap $\delta_f=23°$		Tail off  $i_w = 4°$		5(i)
			-6.0  $i_w = 4°$		
			14.0  $i_w = 4°$		



(a) Front view.

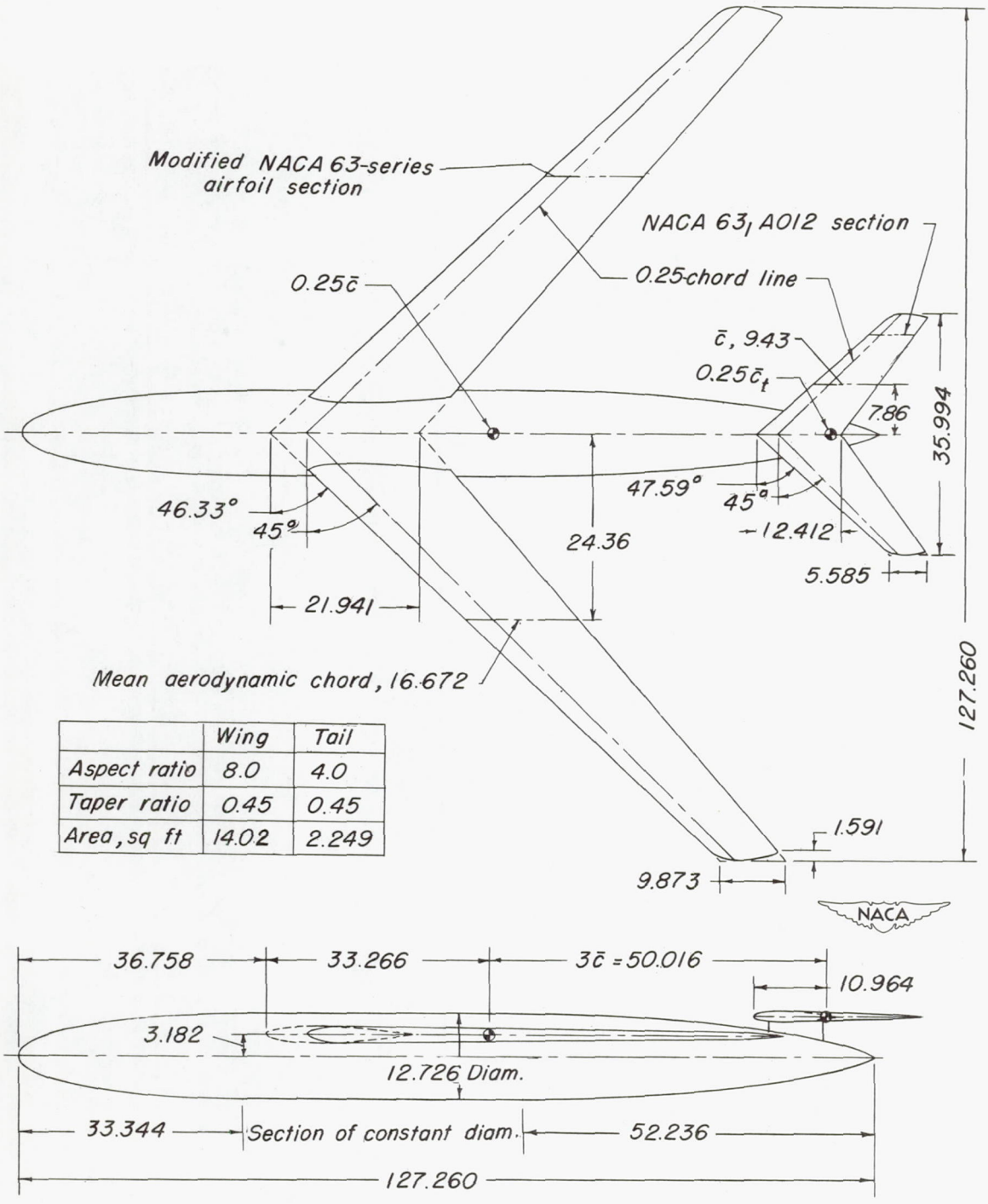
Figure 1.- The twisted and cambered wing-fuselage configuration in combination with a horizontal tail mounted in the Langley 19-foot pressure tunnel. Tail height, 0.14b/2.



(b) Rear view.

Figure 1.- Concluded.

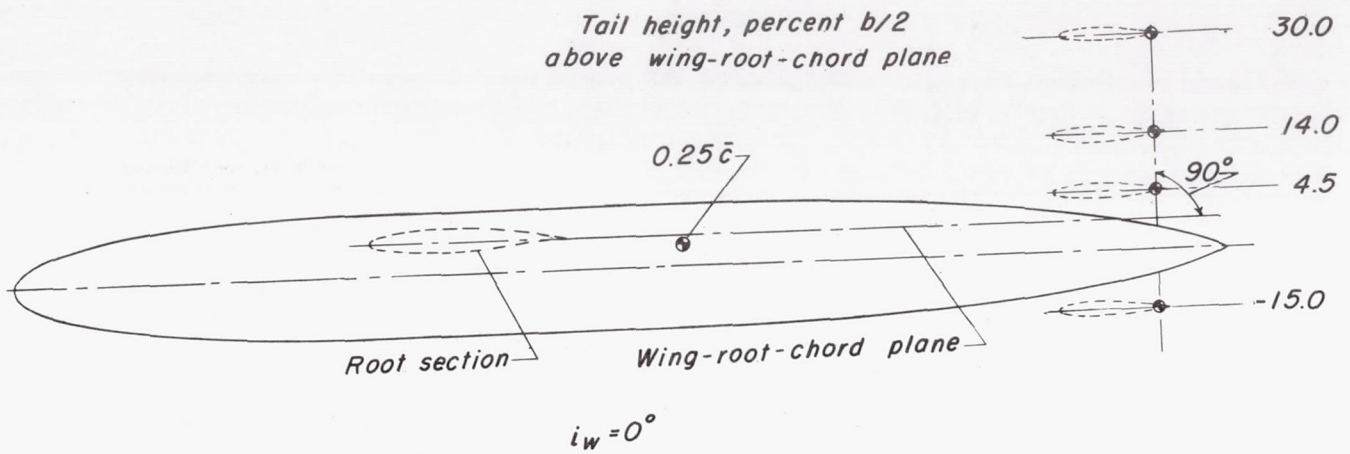
NACA L-71816

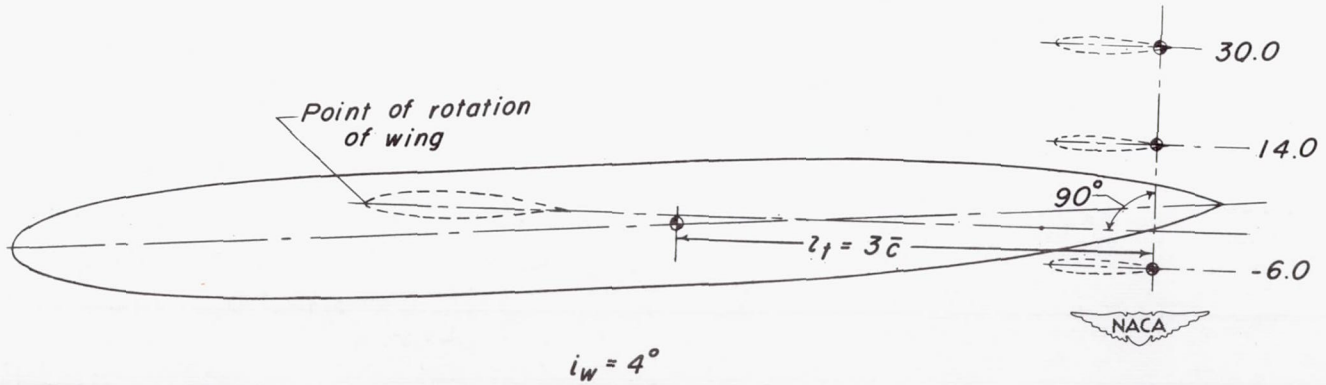


	Wing	Tail
Aspect ratio	8.0	4.0
Taper ratio	0.45	0.45
Area, sq ft	14.02	2.249

(a) Geometry of wing, fuselage, and horizontal tail.

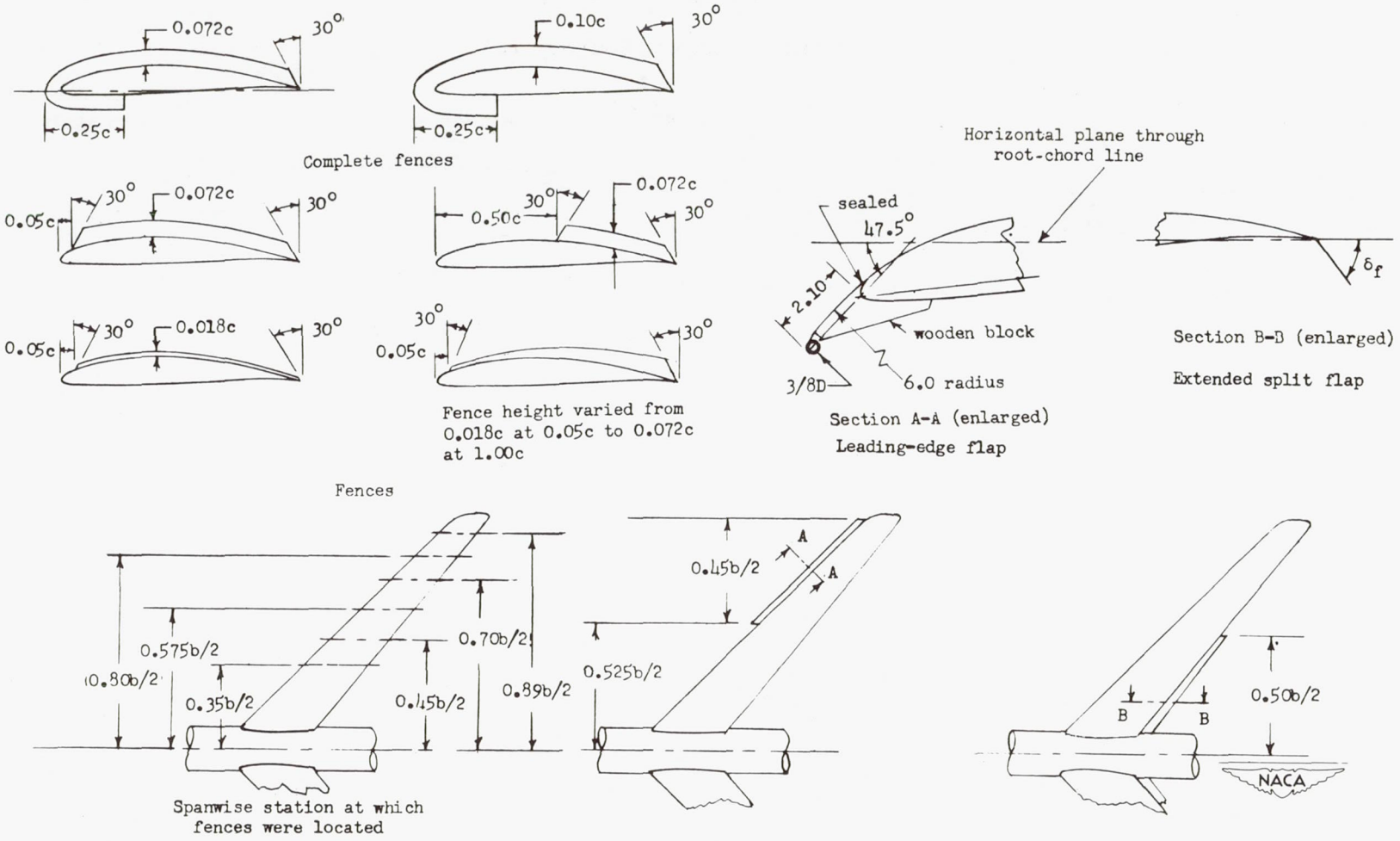
Figure 2.- Model details. All dimensions in inches except where noted.





(b) Horizontal-tail location.

Figure 2.- Continued.



(c) Fences. (d) Leading-edge flaps. (e) Extended split flaps.

Figure 2.- Concluded.

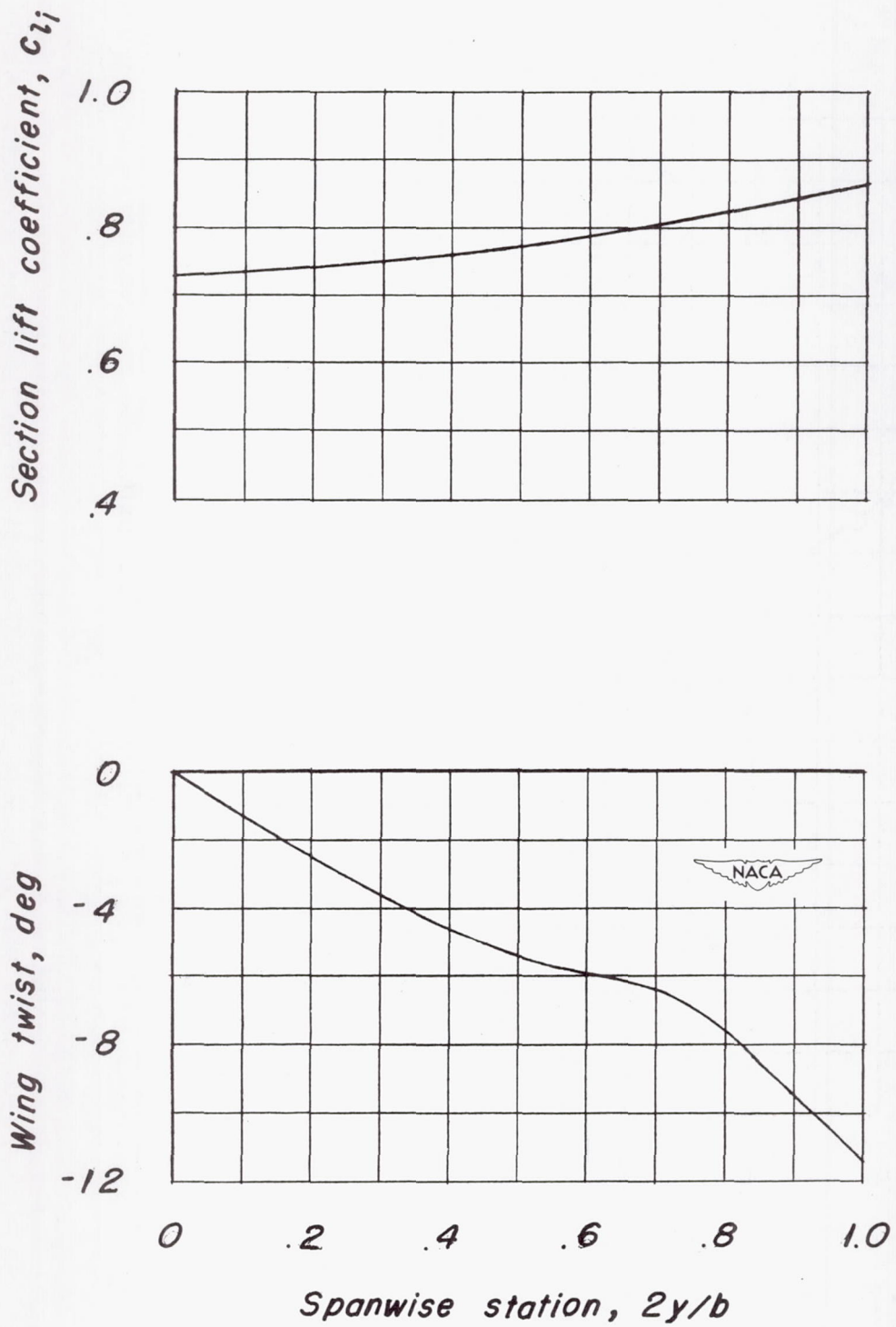


Figure 3.- Spanwise variation of wing twist and distribution of section lift coefficient of the twisted and cambered wing.

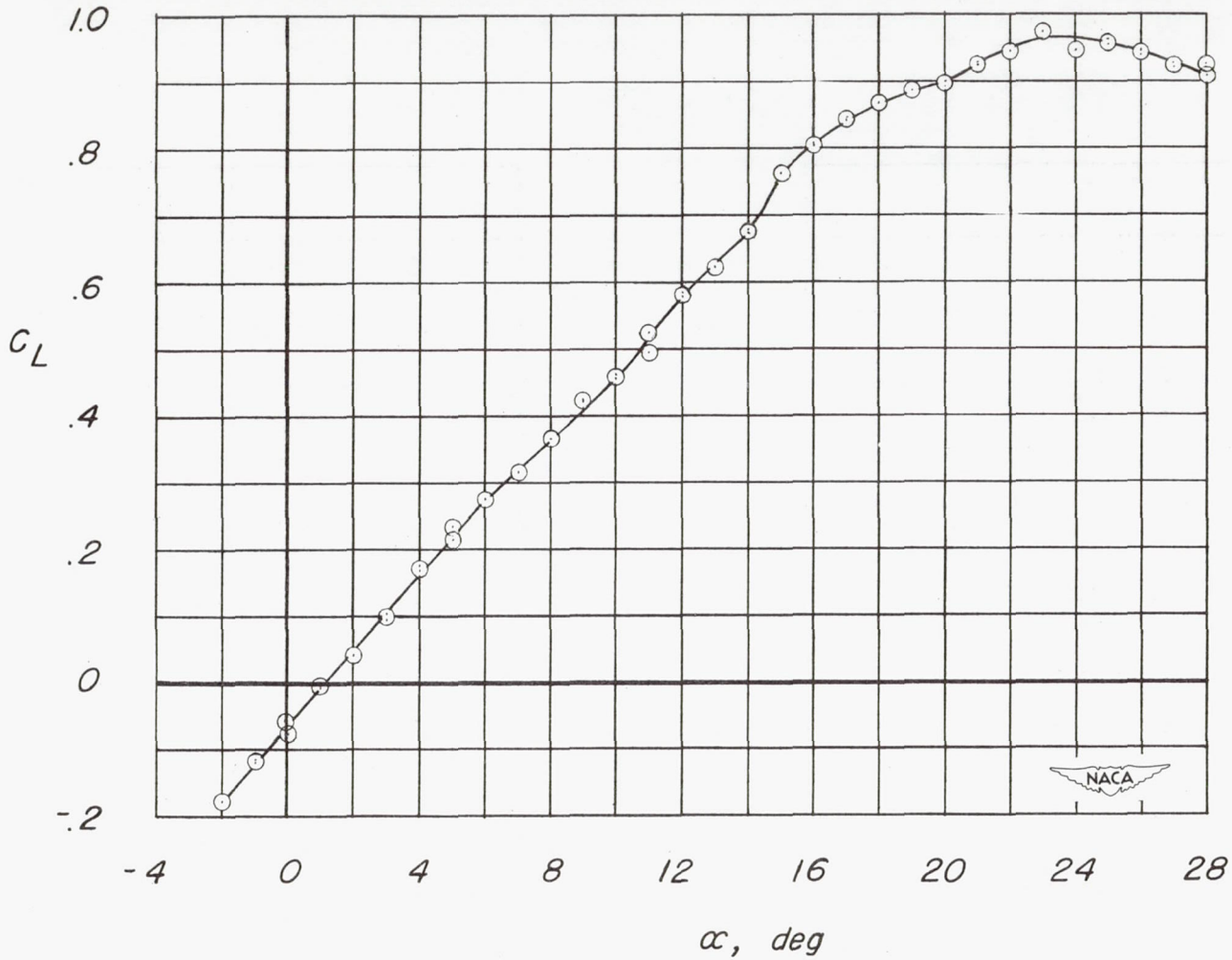
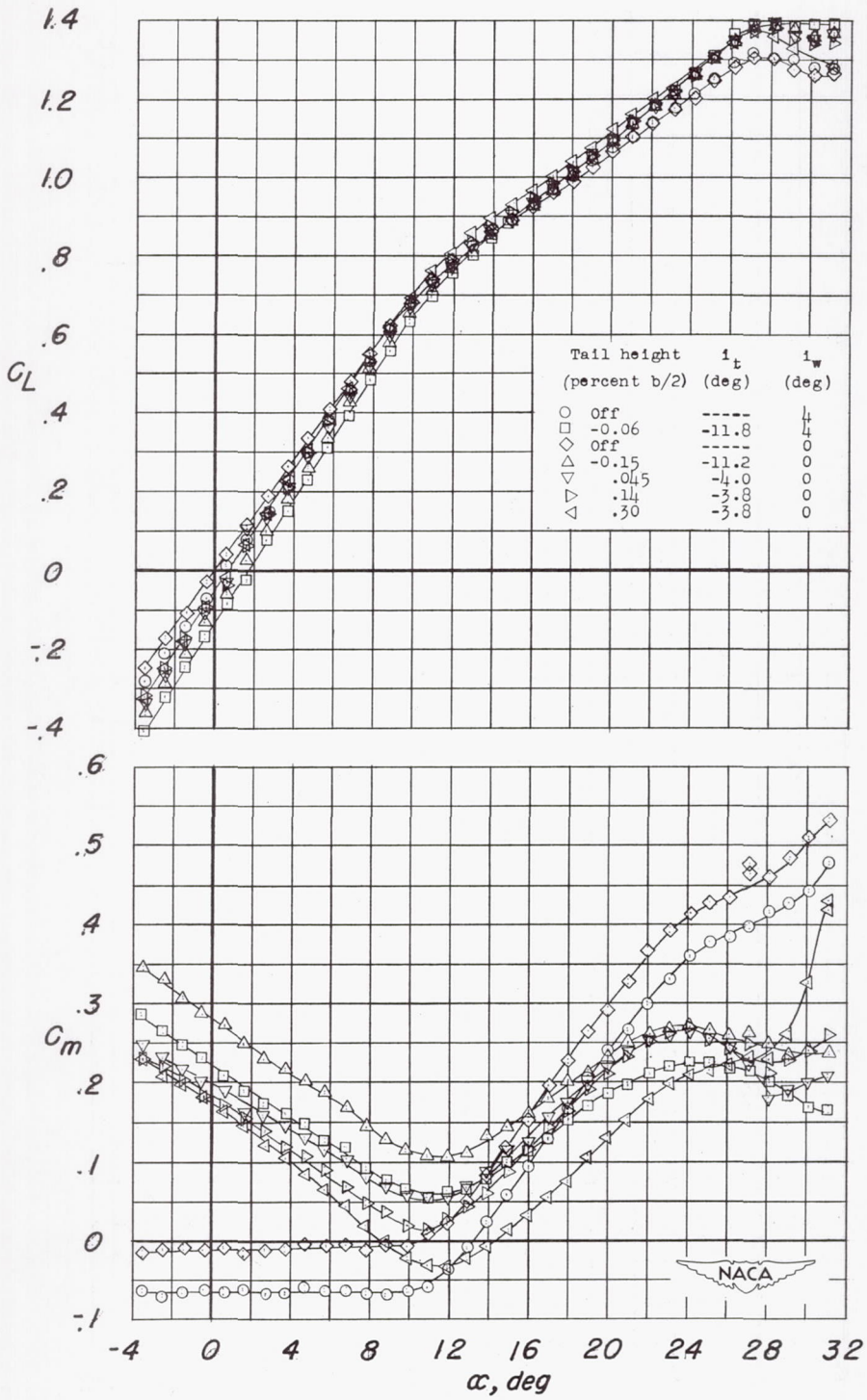
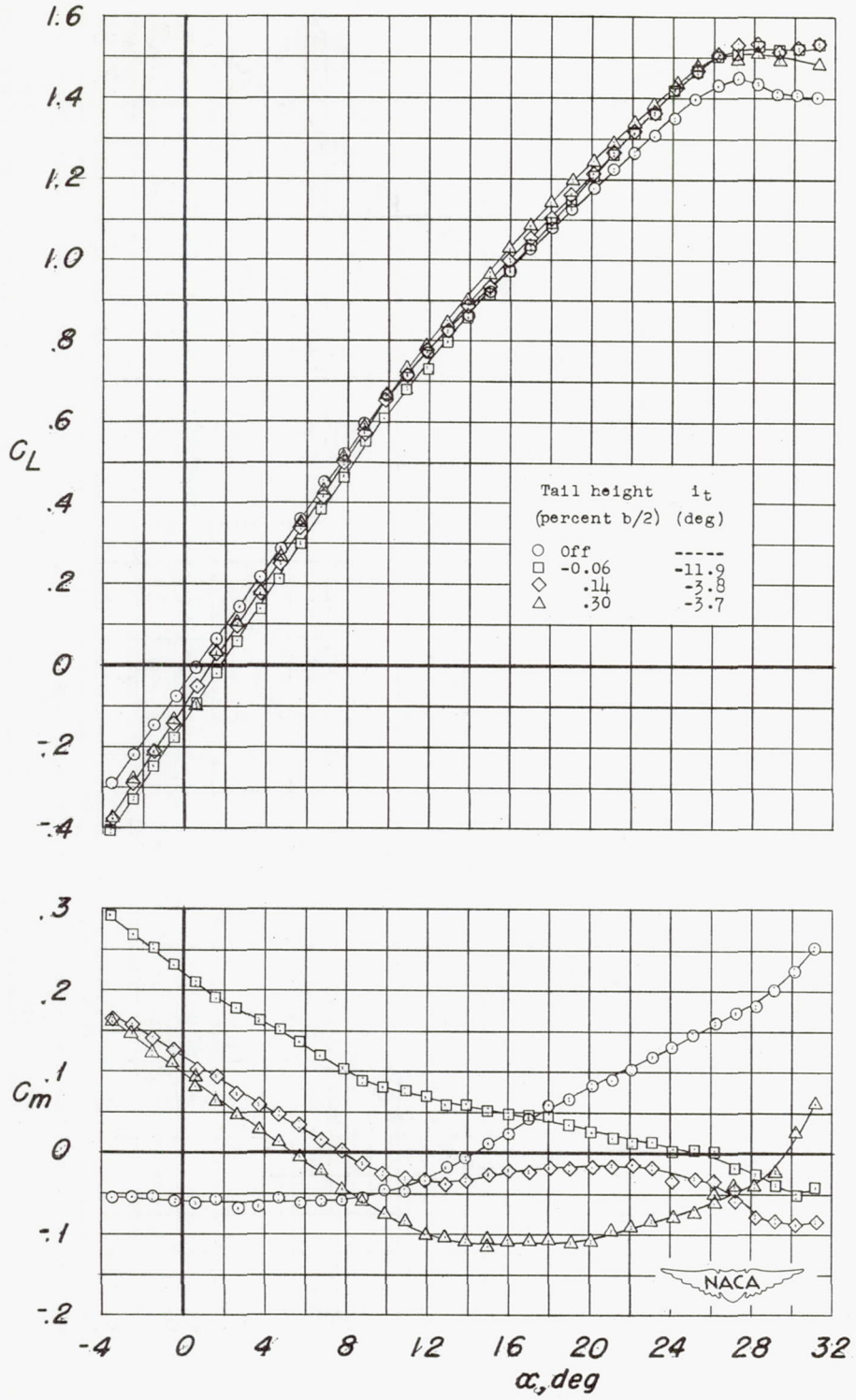


Figure 4.- Variation of lift coefficient with angle of attack of the 45° sweptback tail of aspect ratio 4.0 and NACA 63_1A012 airfoil sections. $R = 2.26 \times 10^6$ corresponding to the wing $R = 4.00 \times 10^6$.



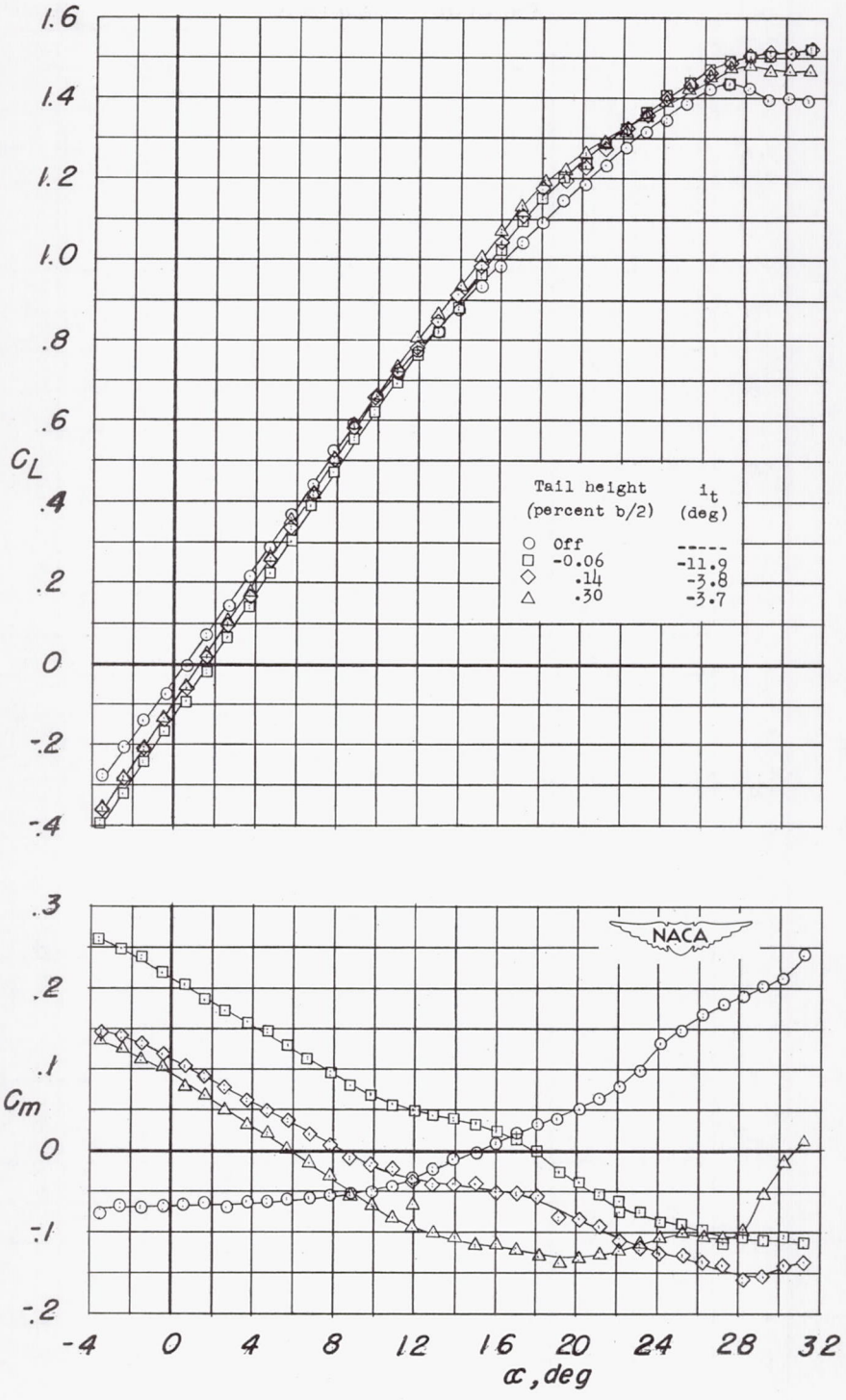
(a) Plain wing.

Figure 5.- Variation of lift coefficient and pitching-moment coefficient with angle of attack for various tail positions.



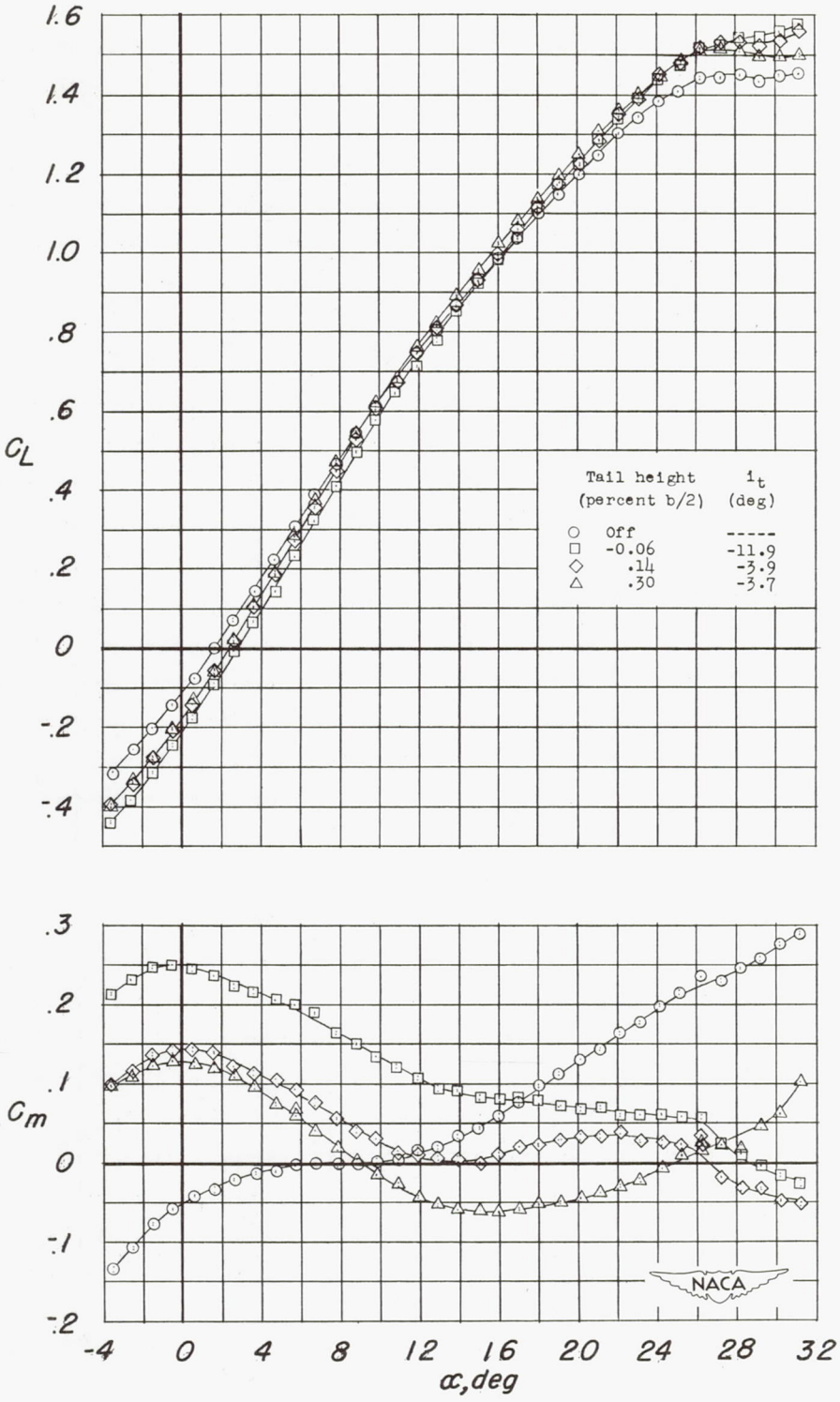
(b) Chord fences located at 0.575b/2 and 0.80b/2; $i_w = 4^\circ$.

Figure 5.- Continued.



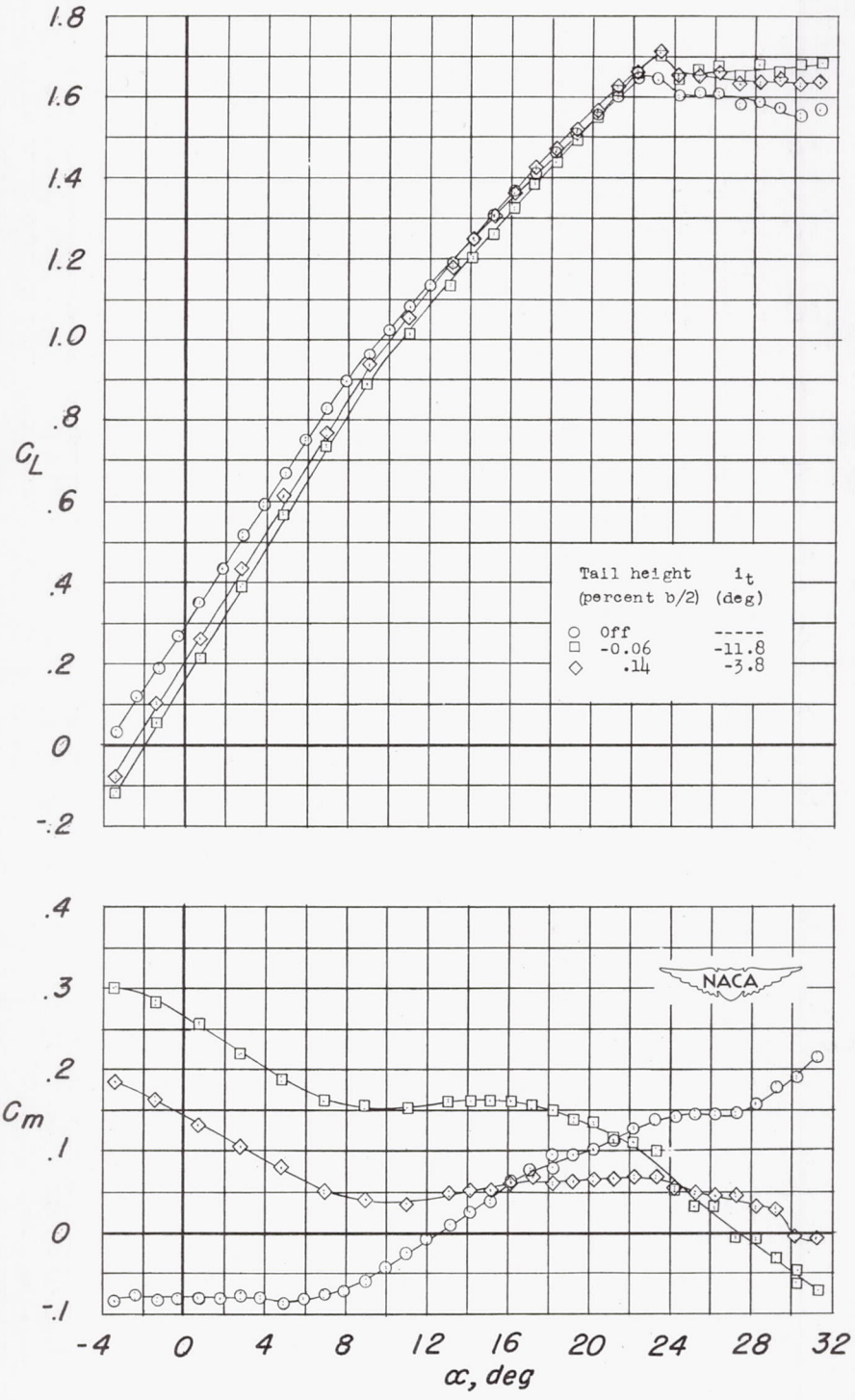
(c) Complete fences located at 0.35b/2, 0.575b/2, and 0.80b/2; chord fences located at 0.89b/2; $i_w = 4^\circ$.

Figure 5.- Continued.



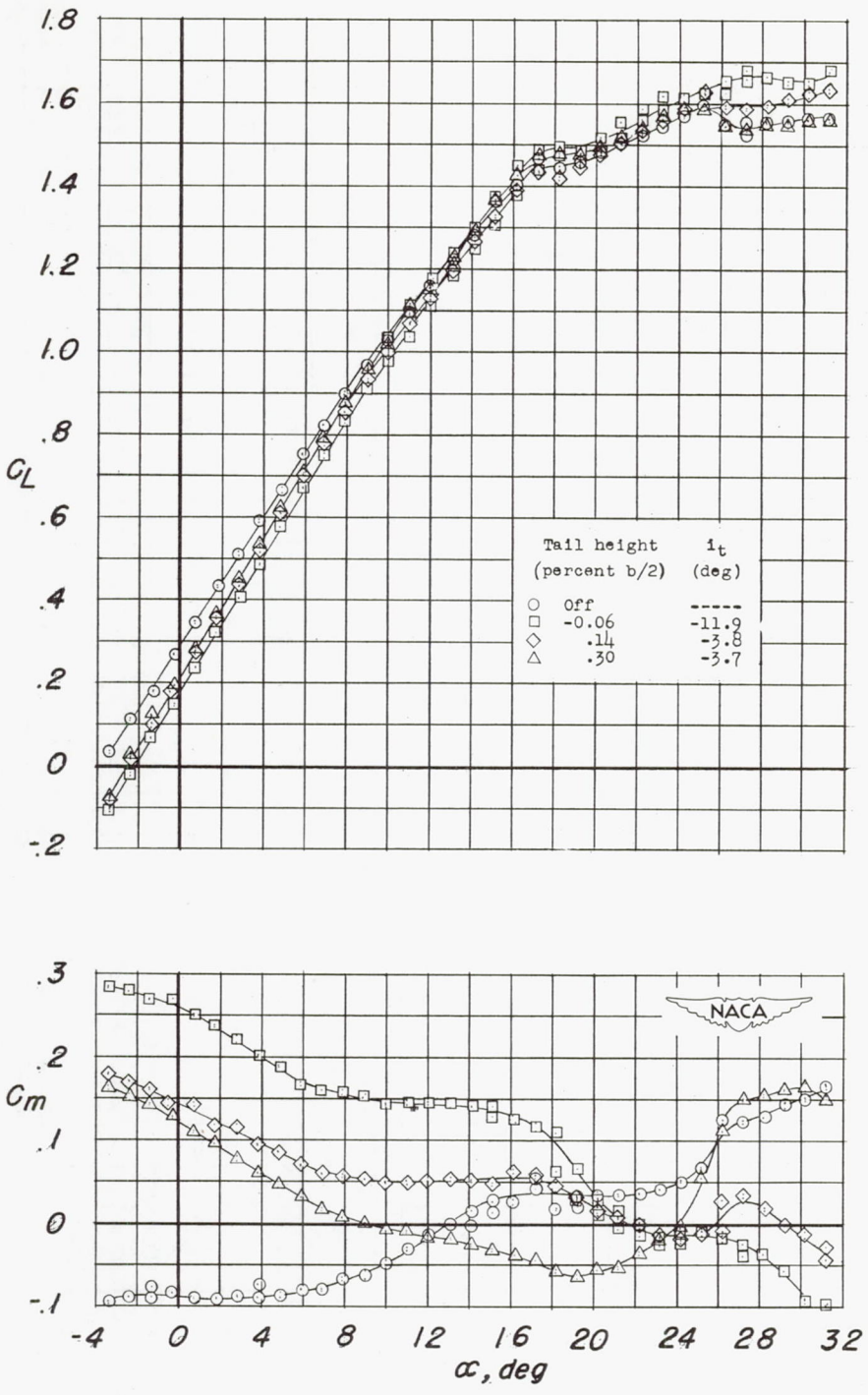
(d) 0.45b/2 leading-edge flaps; $i_w = 4^\circ$.

Figure 5.- Continued.



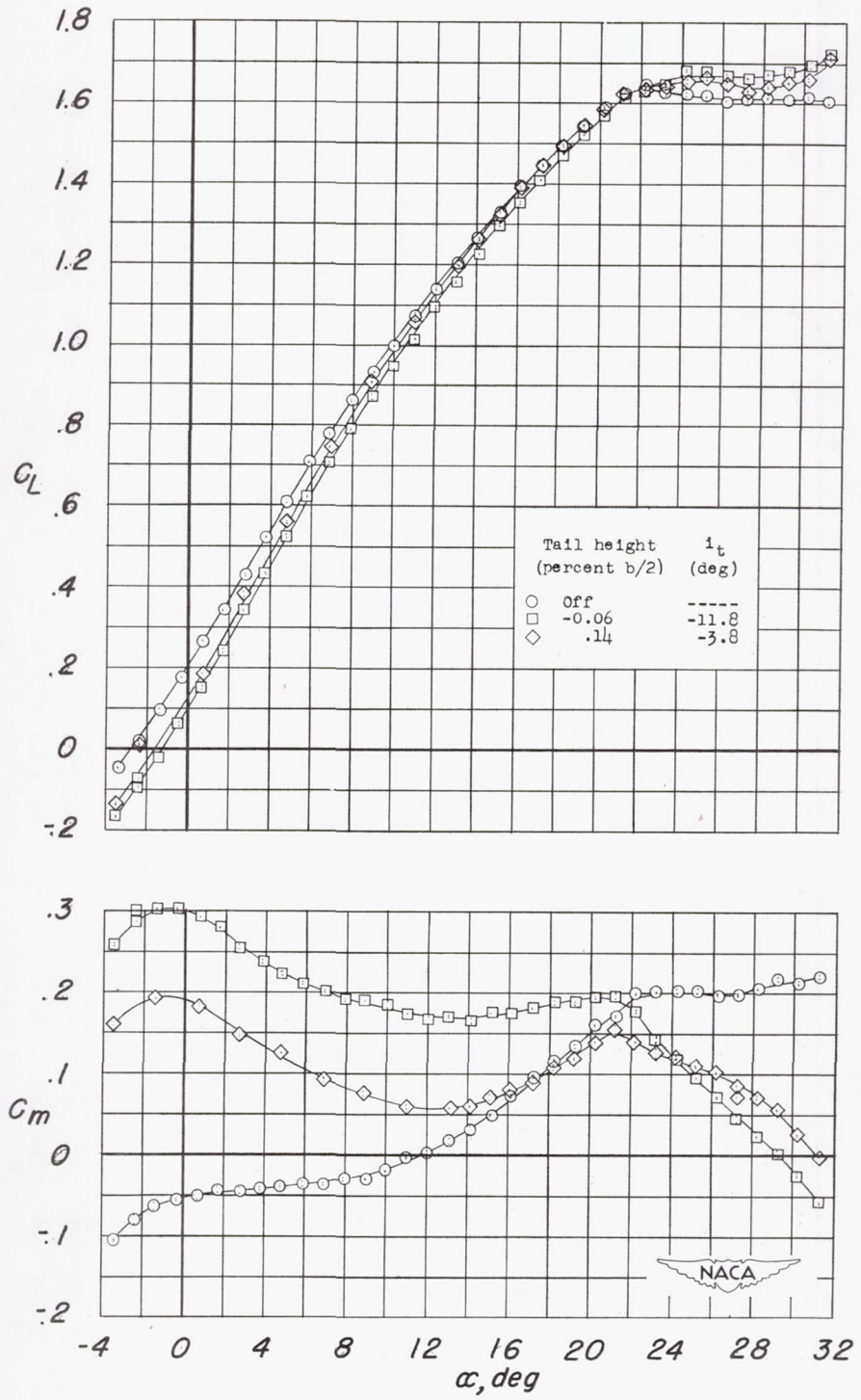
(e) 0.50b/2 extended split flaps (δ_f = 23.3°); chord fences located at 0.575b/2 and 0.80b/2; i_w = 4°.

Figure 5.- Continued.



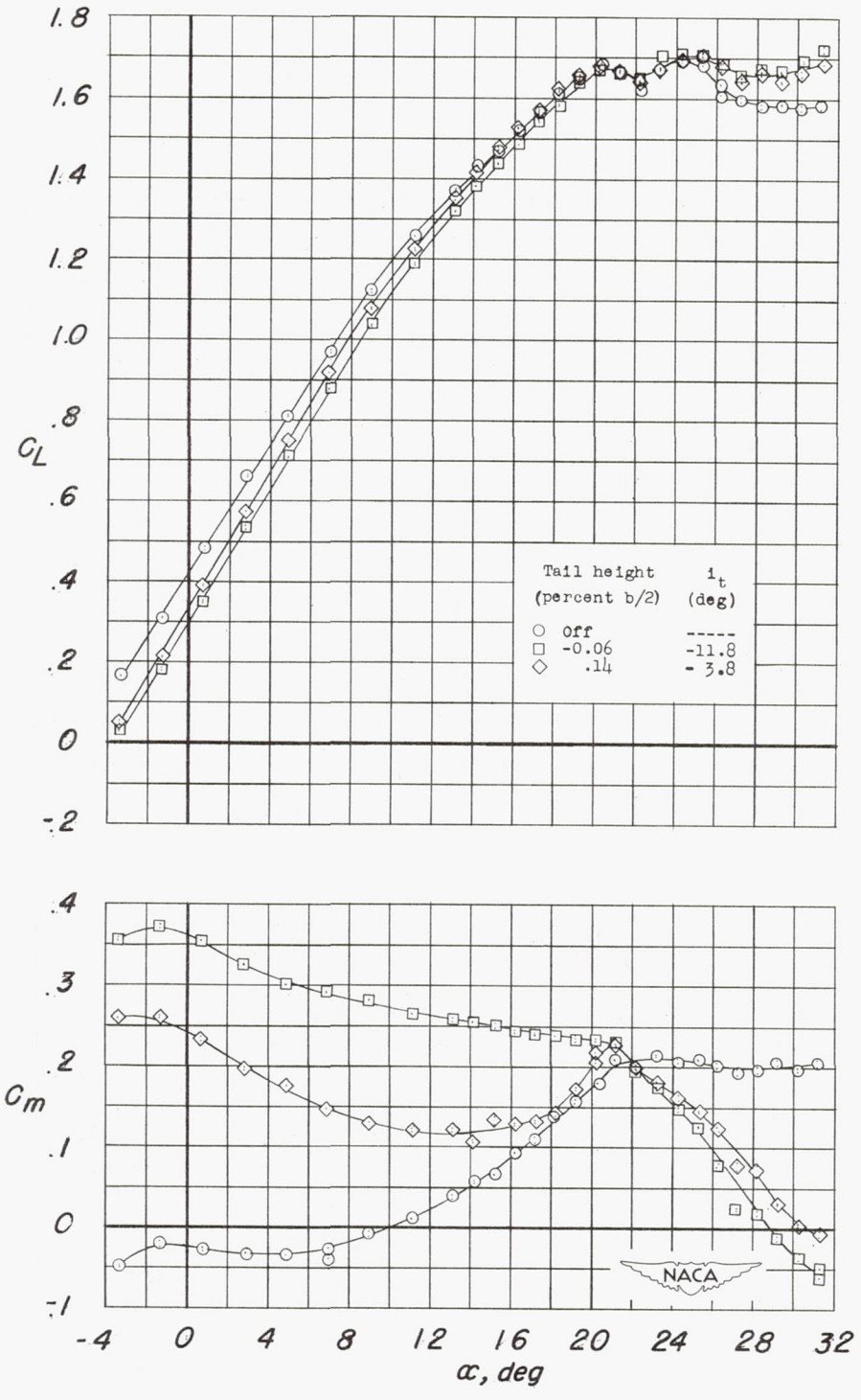
(f) 0.50b/2 extended split flaps (δ_f = 23°); complete fence located at 0.35b/2, 0.575b/2, and 0.80b/2; chord fences located at 0.89b/2; i_w = 4°.

Figure 5.- Continued.



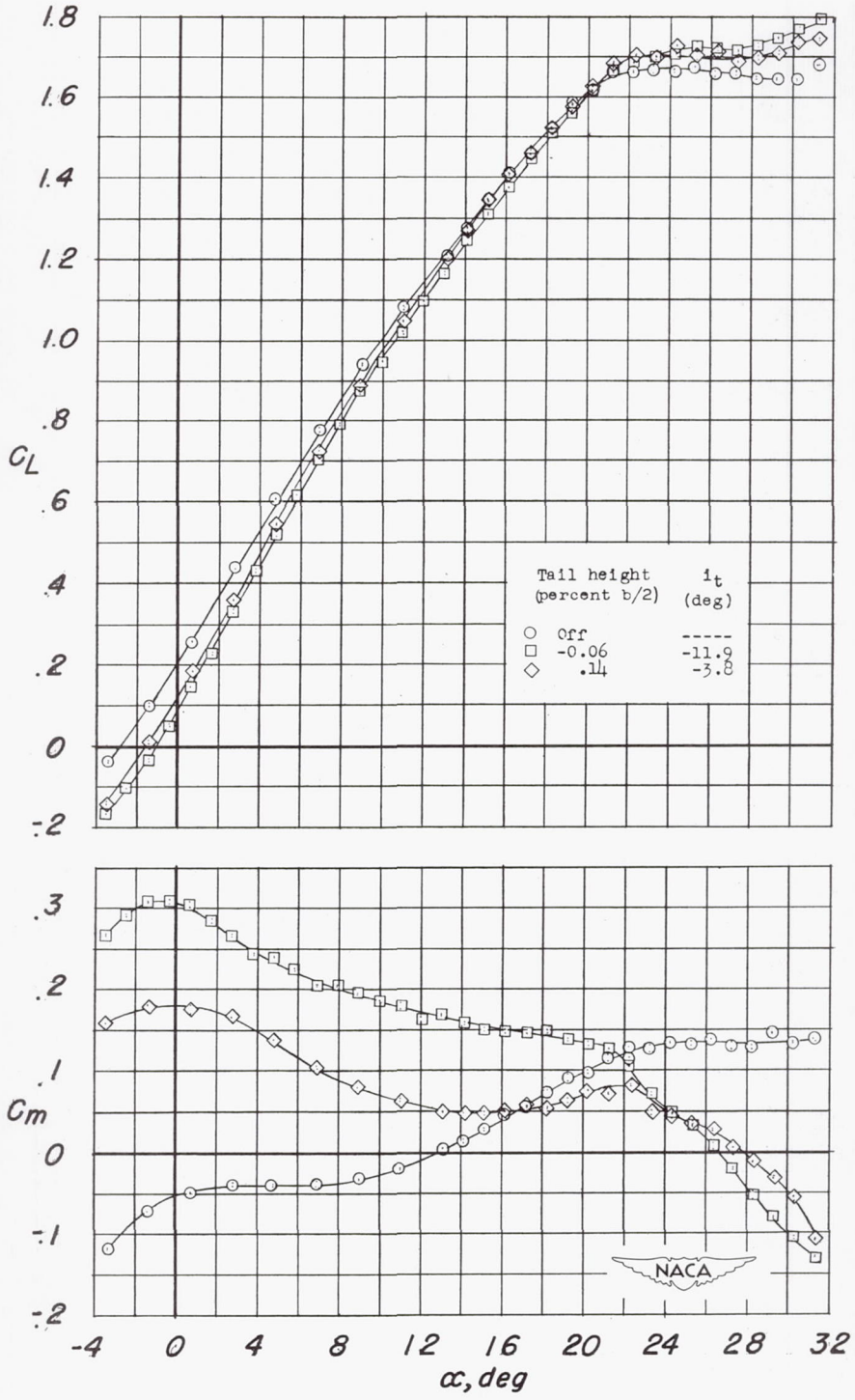
(g) 0.45b/2 leading-edge flaps and 0.50b/2 extended split flaps ($\delta_f = 23^\circ$); $i_w = 4^\circ$.

Figure 5.- Continued.



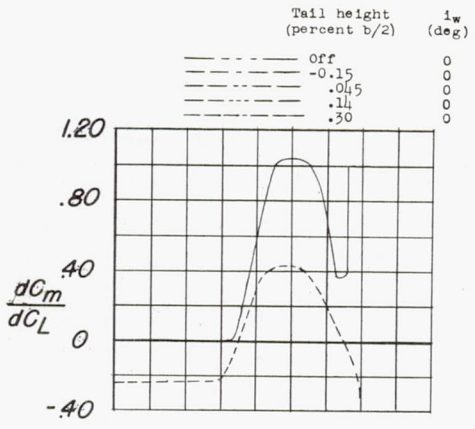
(h) 0.45b/2 leading-edge flaps and 0.50b/2 extended split flaps ($\delta_f = 52^\circ$); $i_w = 4^\circ$.

Figure 5.- Continued.

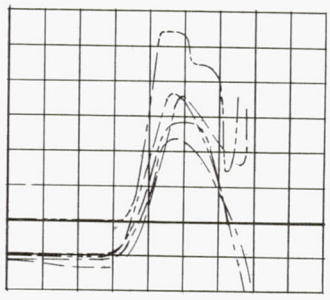


(i) 0.45b/2 leading-edge flaps; 0.50b/2 extended split flaps ($\delta_f = 23^\circ$); chord fences located at 0.575b/2 and 0.80b/2; $i_w = 4^\circ$.

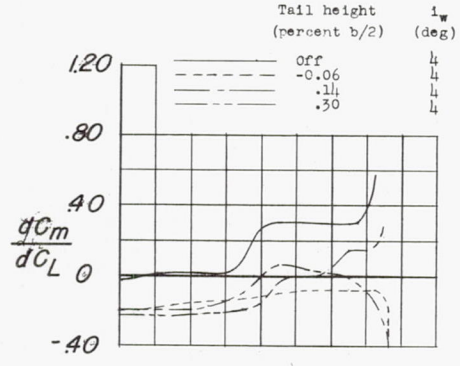
Figure 5.- Concluded.



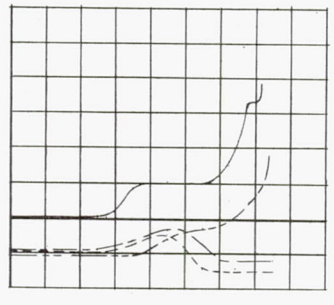
(a) Plain wing; $i_w = 4^\circ$.



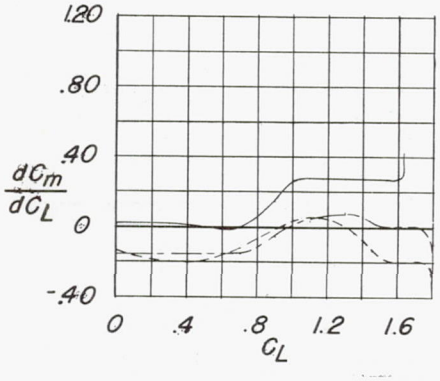
(b) Plain wing; $i_w = 0^\circ$.



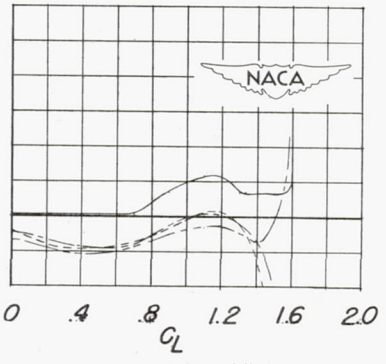
(c) Chord fences located at 0.575b/2 and 0.80b/2; $i_w = 4^\circ$.



(d) Complete fences located at 0.35b/2, 0.575b/2, and 0.80b/2; chord fences located at 0.89b/2; $i_w = 4^\circ$.

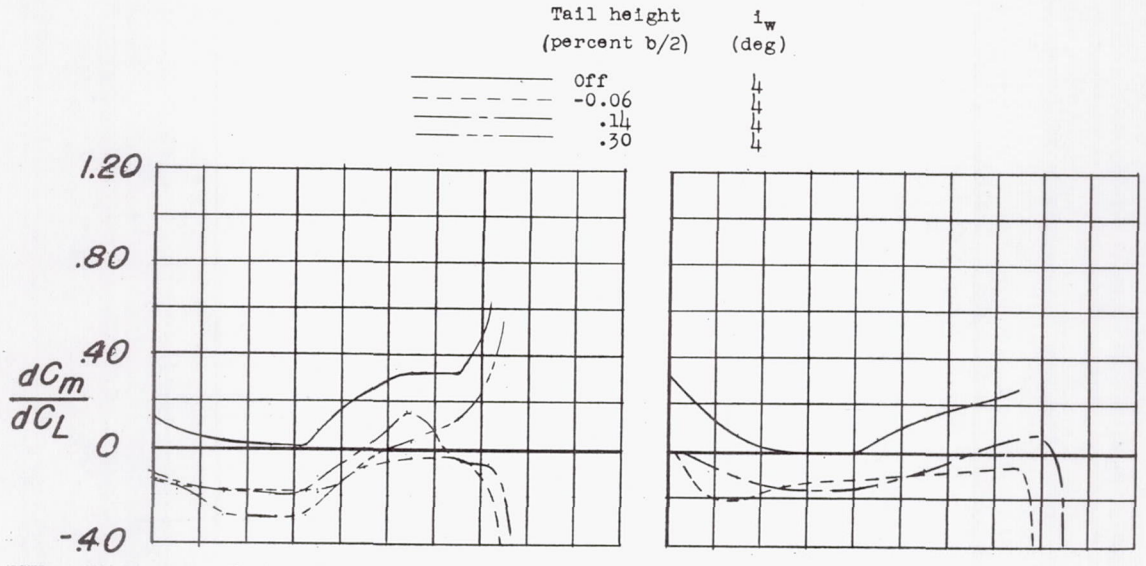


(e) 0.50b/2 extended split flaps ($\delta_f = 23^\circ$); chord fences located at 0.575b/2 and 0.80b/2; $i_w = 4^\circ$.



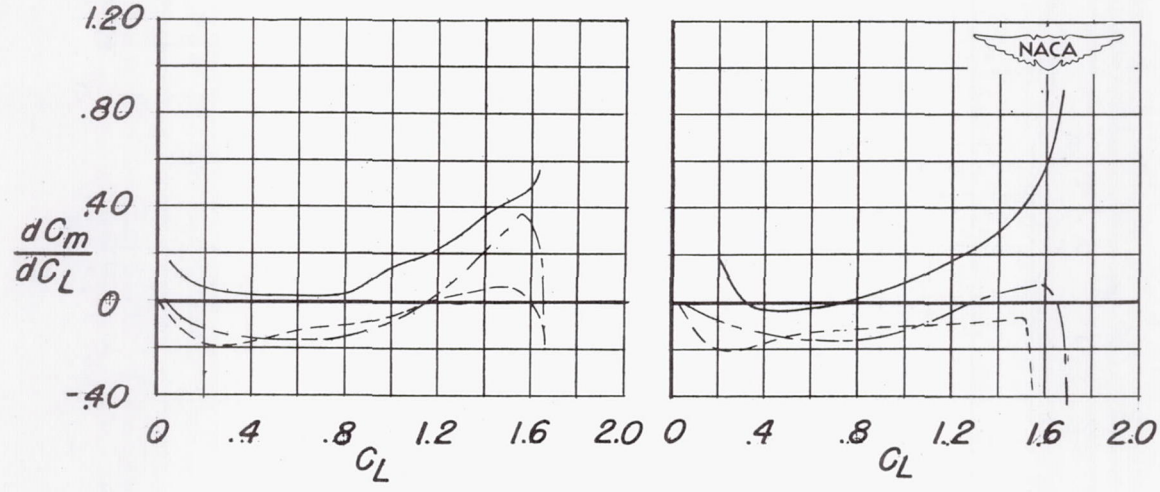
(f) 0.50b/2 extended split flaps ($\delta_f = 23^\circ$); complete fence located at 0.35b/2, 0.575b/2, and 0.80b/2; chord fences located at 0.89b/2; $i_w = 4^\circ$.

Figure 6.- Variation of dC_m/dC_L of the wing-fuselage combination with and without the horizontal tail.



(g) 0.45b/2 leading-edge flaps, $i_w = 4^\circ$.

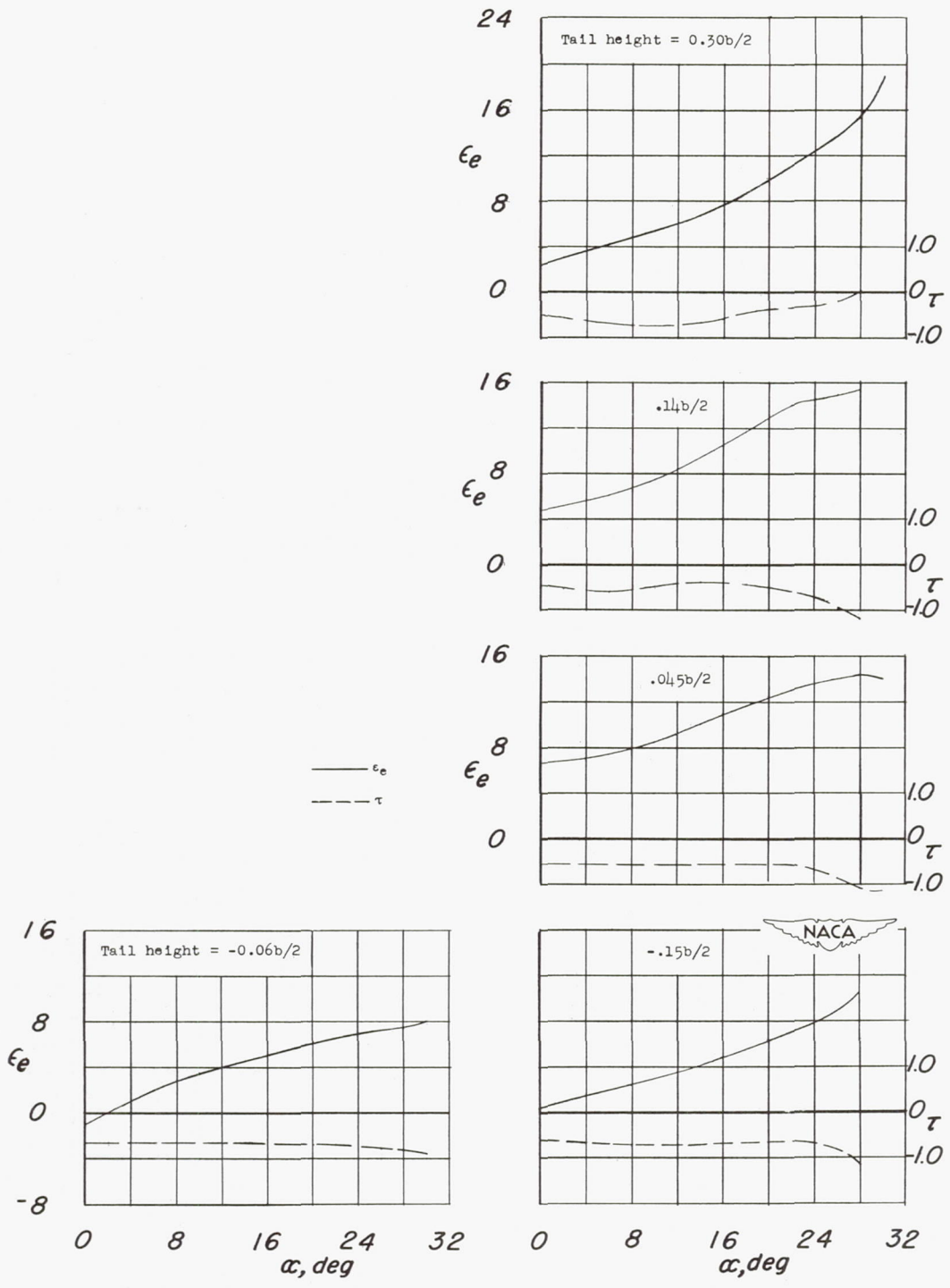
(h) 0.45b/2 leading-edge flaps; 0.50b/2 extended split flaps ($\delta_f = 23^\circ$); chord fences located at 0.575b/2 and 0.80b/2; $i_w = 4^\circ$.



(i) 0.45b/2 leading-edge flaps and 0.50b/2 extended split flaps ($\delta_f = 23^\circ$); $i_w = 4^\circ$.

(j) 0.45b/2 leading-edge flaps and 0.50b/2 extended split flaps ($\delta_f = 52^\circ$); $i_w = 4^\circ$.

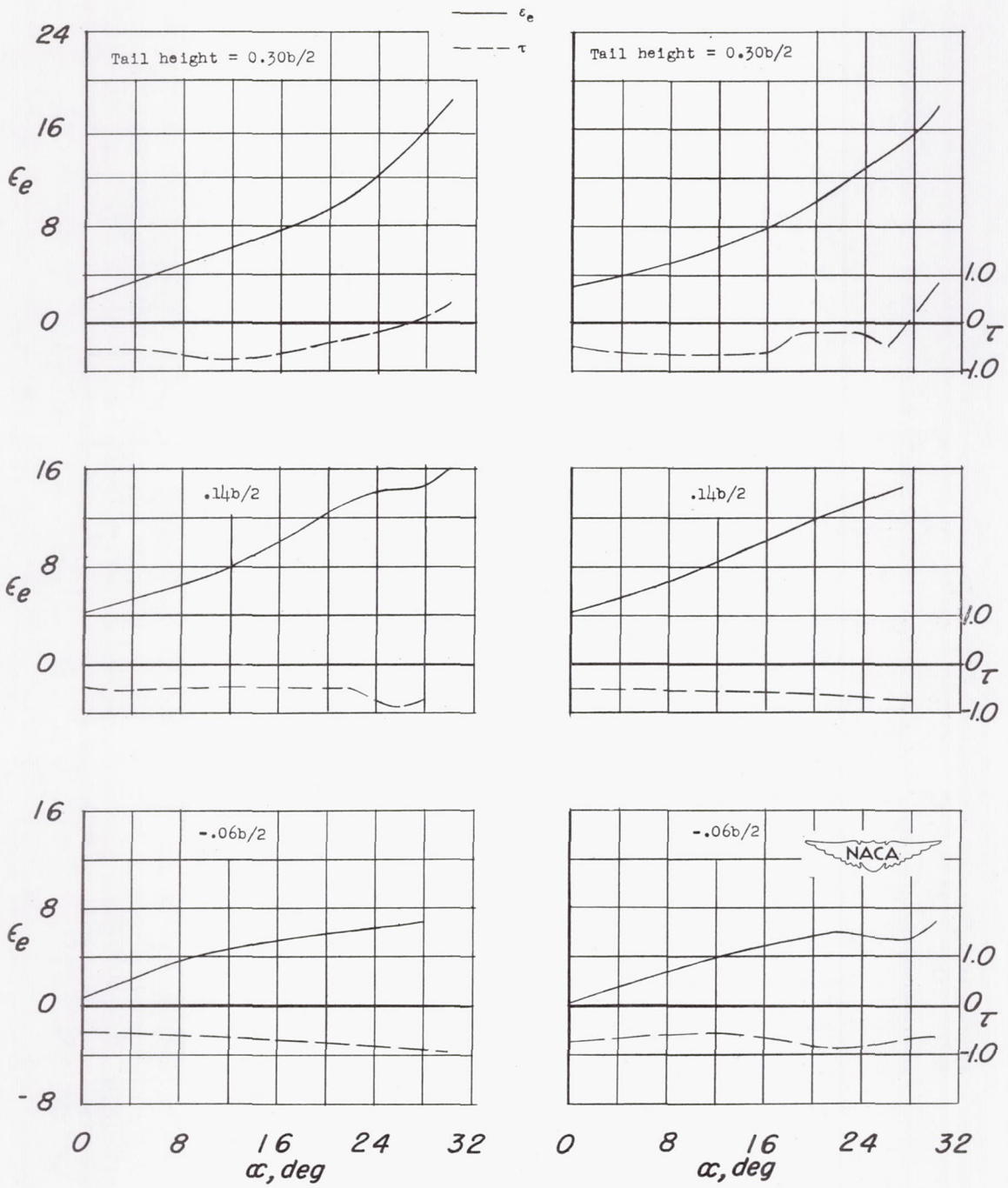
Figure 6.- Concluded.



(a) Plain wing, $i_w = 4^\circ$.

(b) Plain wing, $i_w = 0^\circ$.

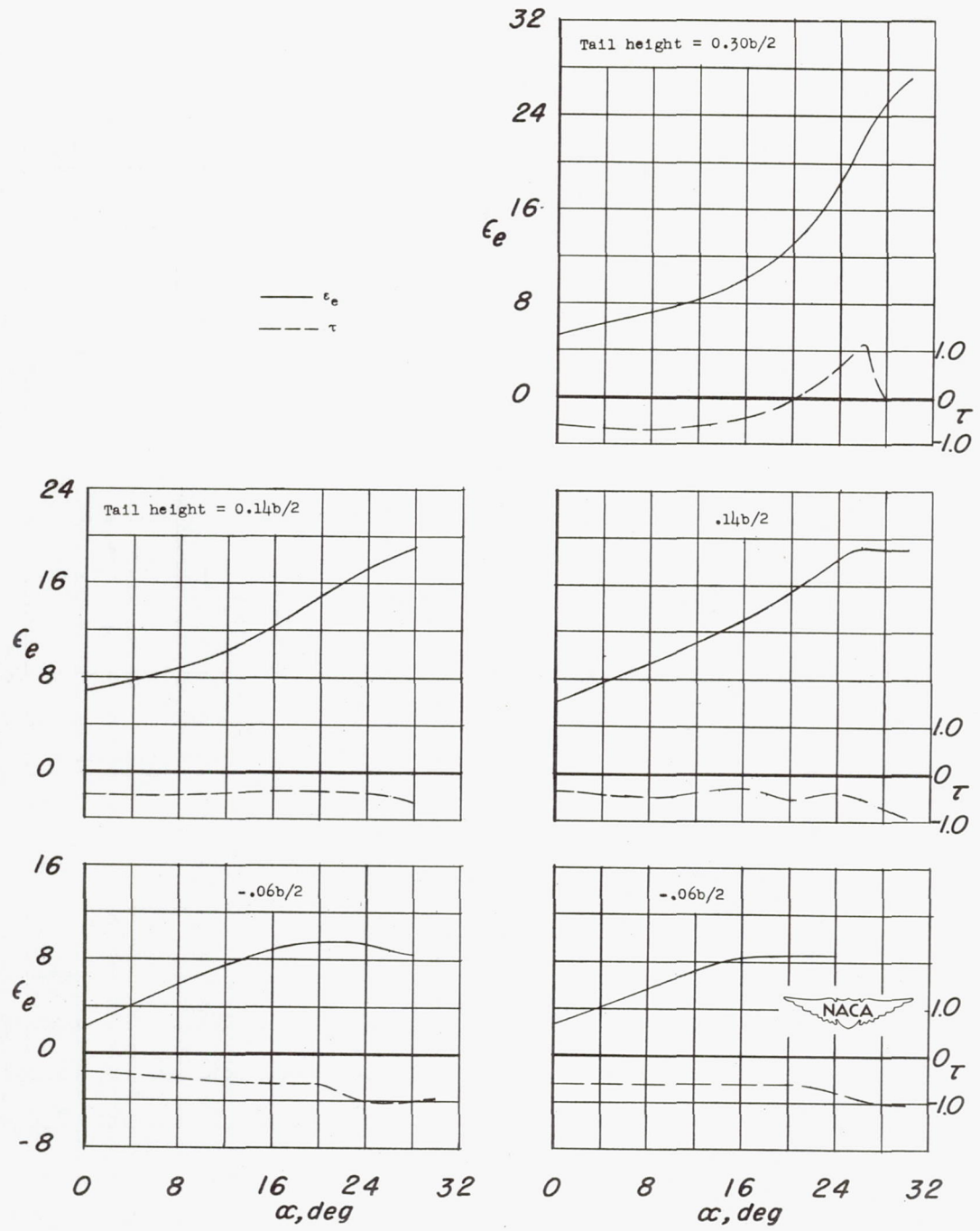
Figure 7.- Variation of effective downwash angle and horizontal-tail-effectiveness parameter τ with angle of attack.



(c) Chord fences located at 0.575b/2 and 0.80b/2; $i_w = 4^\circ$.

(d) Complete fences located at 0.35b/2, 0.575b/2, and 0.80b/2; chord fences located at 0.89b/2; $i_w = 4^\circ$.

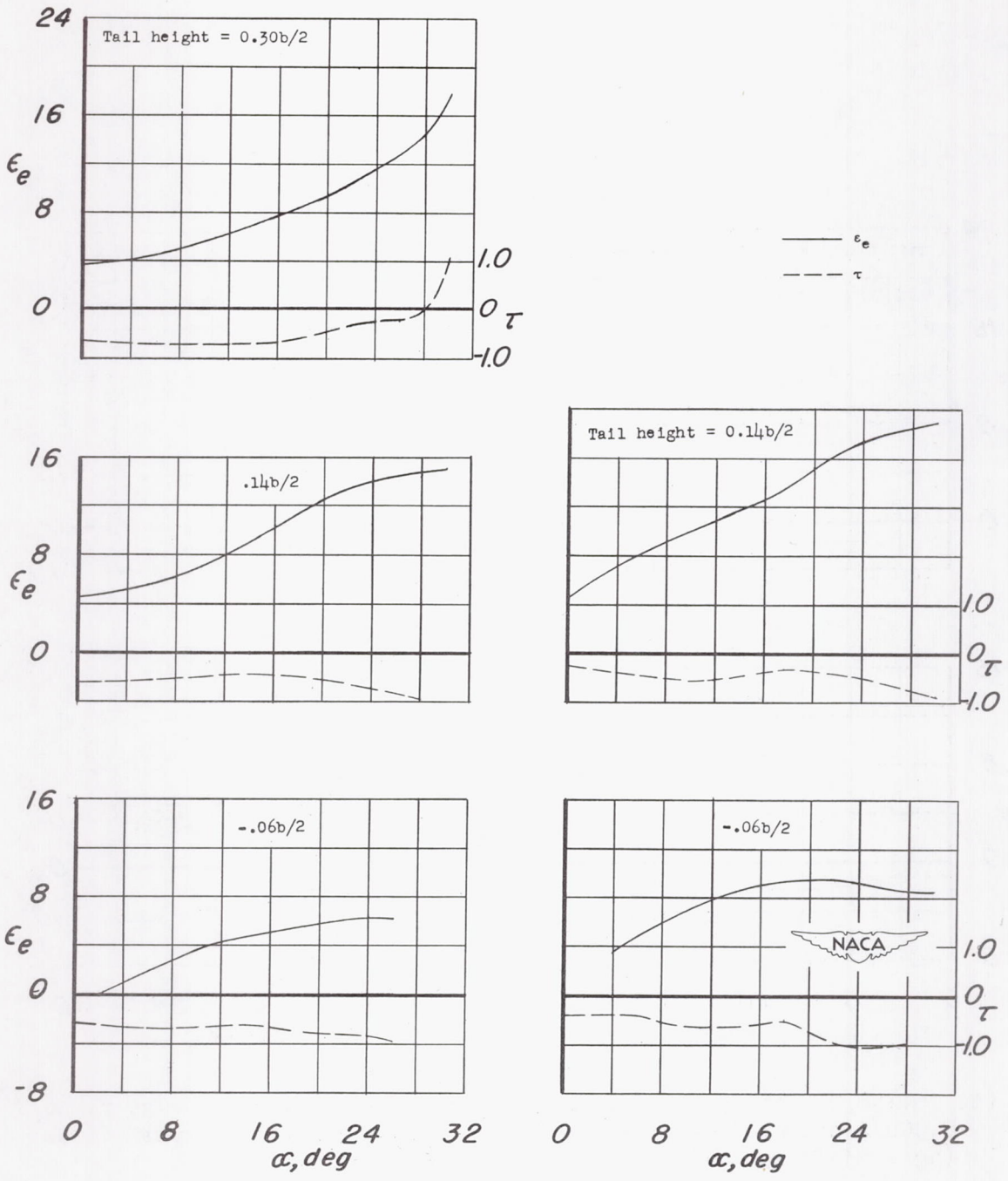
Figure 7.- Continued.



(e) 0.50b/2 extended split flaps ($\delta_f = 23^\circ$); chord fences located at 0.575b/2 and 0.80b/2; $i_w = 4^\circ$.

(f) 0.50b/2 extended split flaps ($\delta_f = 23^\circ$); complete fences located at 0.35b/2, 0.575b/2, and 0.80b/2; chord fences located at 0.89b/2; $i_w = 4^\circ$.

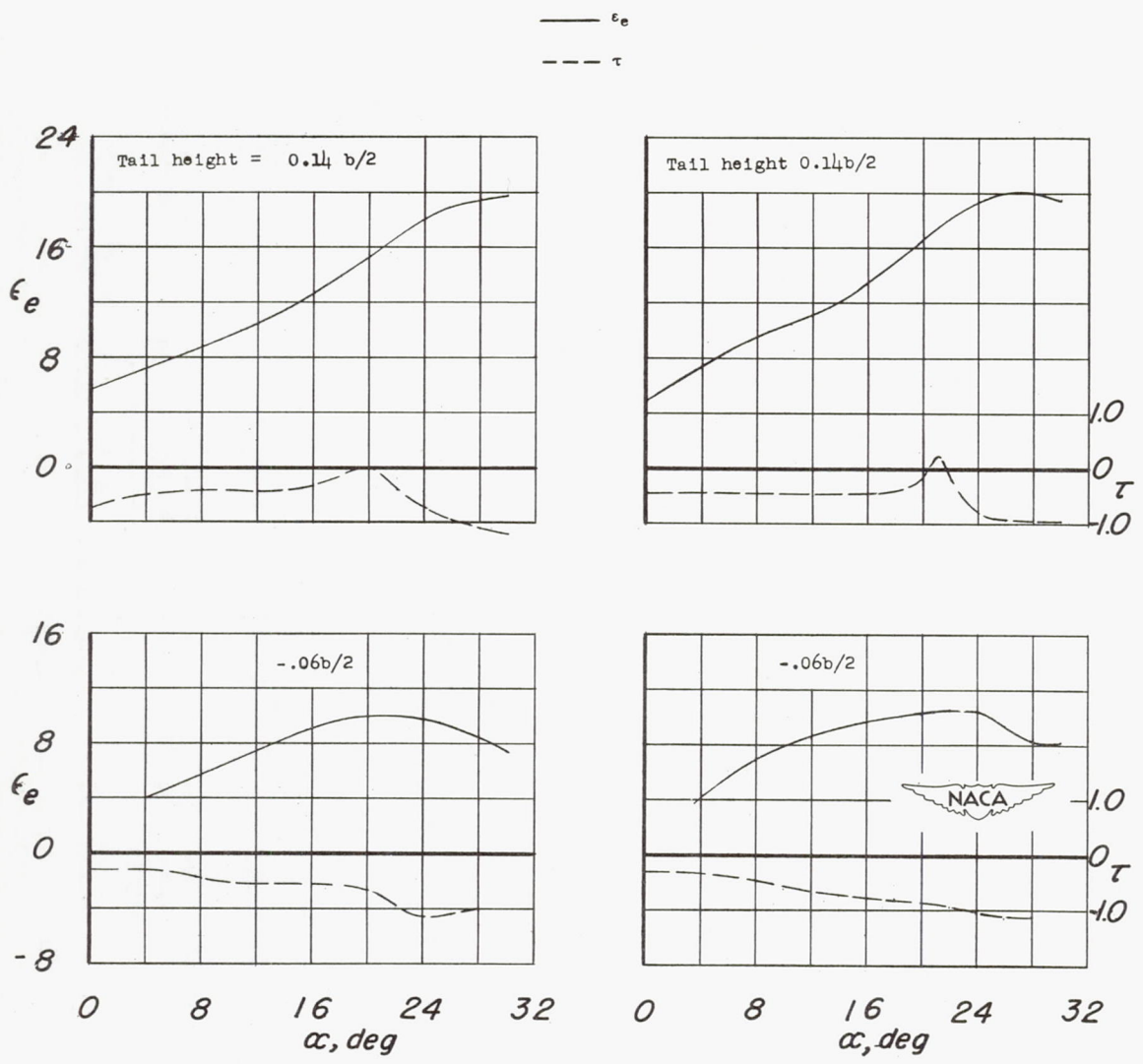
Figure 7.- Continued.



(g) 0.45b/2 leading-edge flaps; $i_w = 4^\circ$.

(h) 0.45b/2 leading-edge flaps; 0.50b/2 extended split flaps ($\delta_f = 23^\circ$); chord fences located at 0.575b/2 and 0.80b/2; $i_w = 4^\circ$.

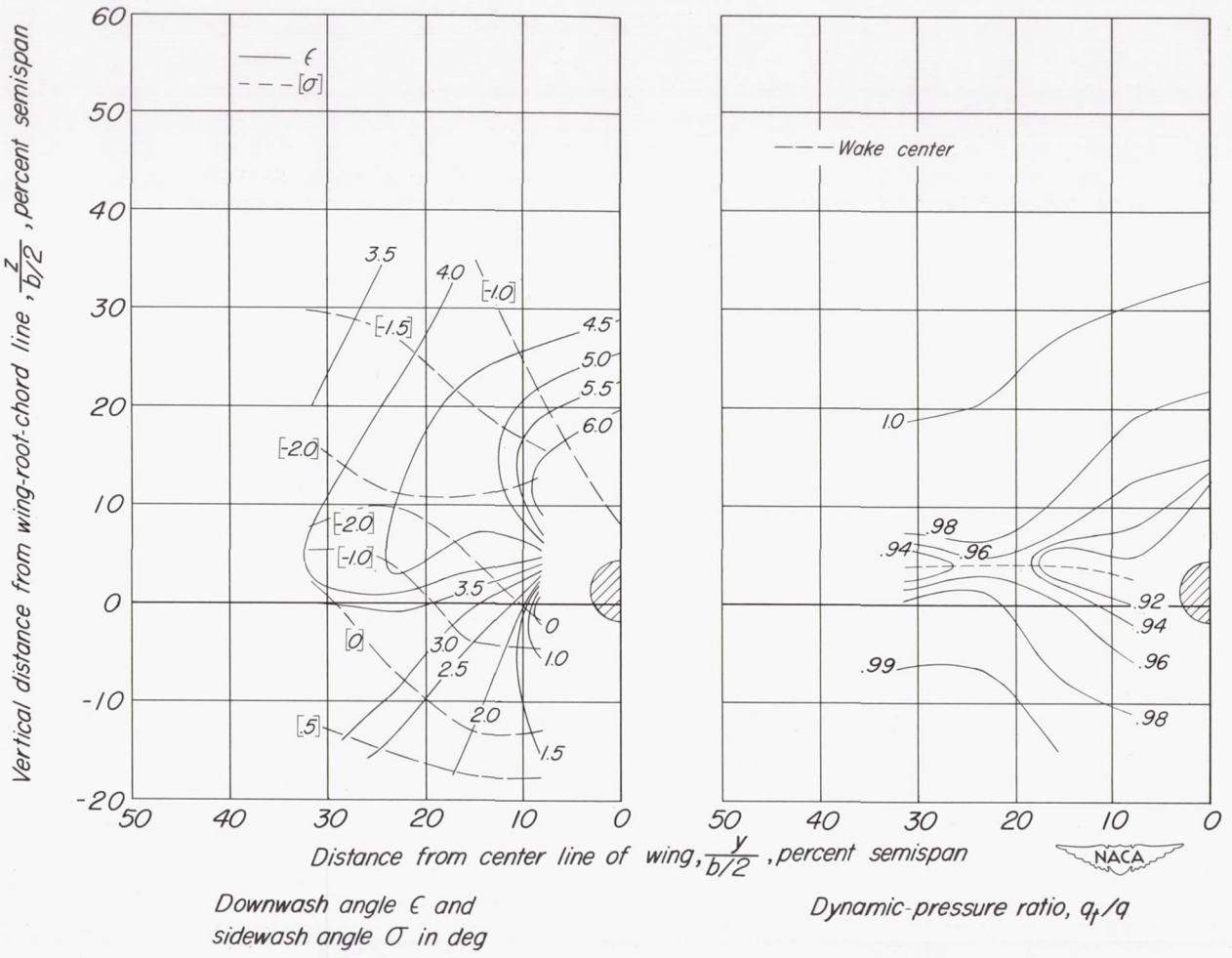
Figure 7.- Continued.



(i) 0.45b/2 leading-edge flaps; 0.50b/2 extended split flaps ($\delta_f = 23^\circ$); $i_w = 4^\circ$.

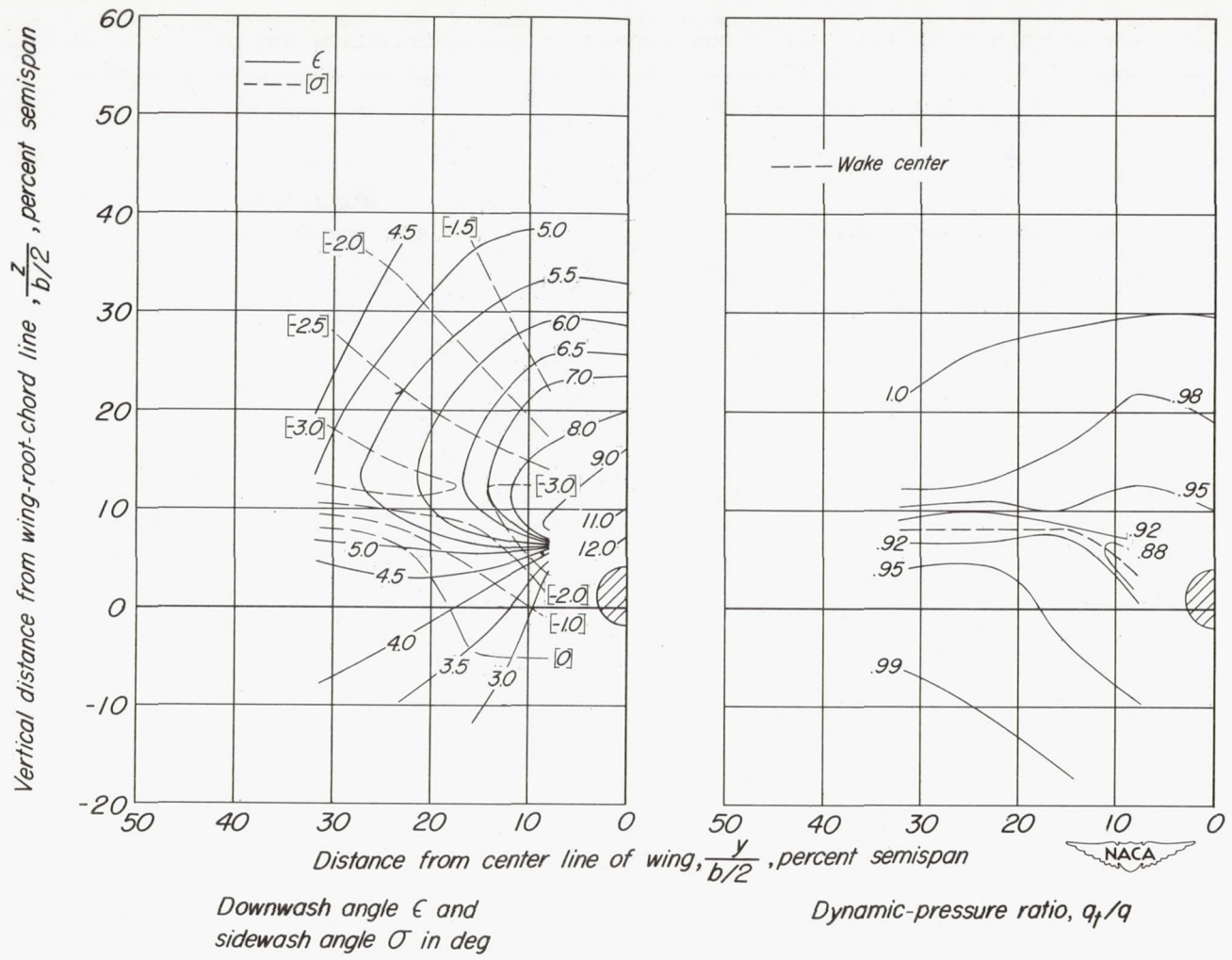
(j) 0.45b/2 leading-edge flaps; 0.50b/2 extended split flaps ($\delta_f = 52^\circ$); $i_w = 4^\circ$.

Figure 7.- Concluded.



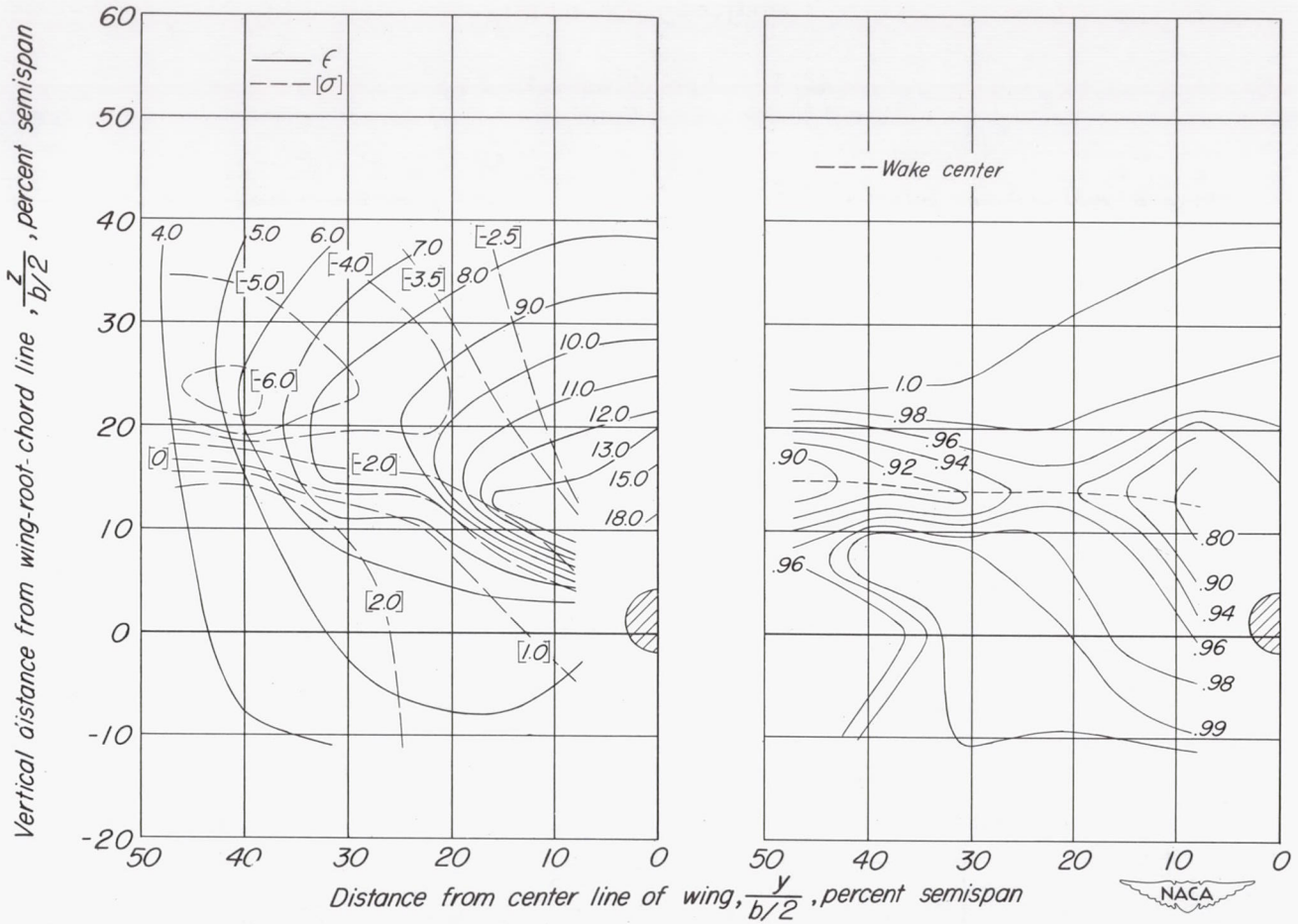
(a) $\alpha = 8.8^{\circ}$; $C_L = 0.60$.

Figure 8.- Contour charts of the air-flow characteristics in the region of the horizontal tail. Fences and flaps off; $i_w = 4^{\circ}$.



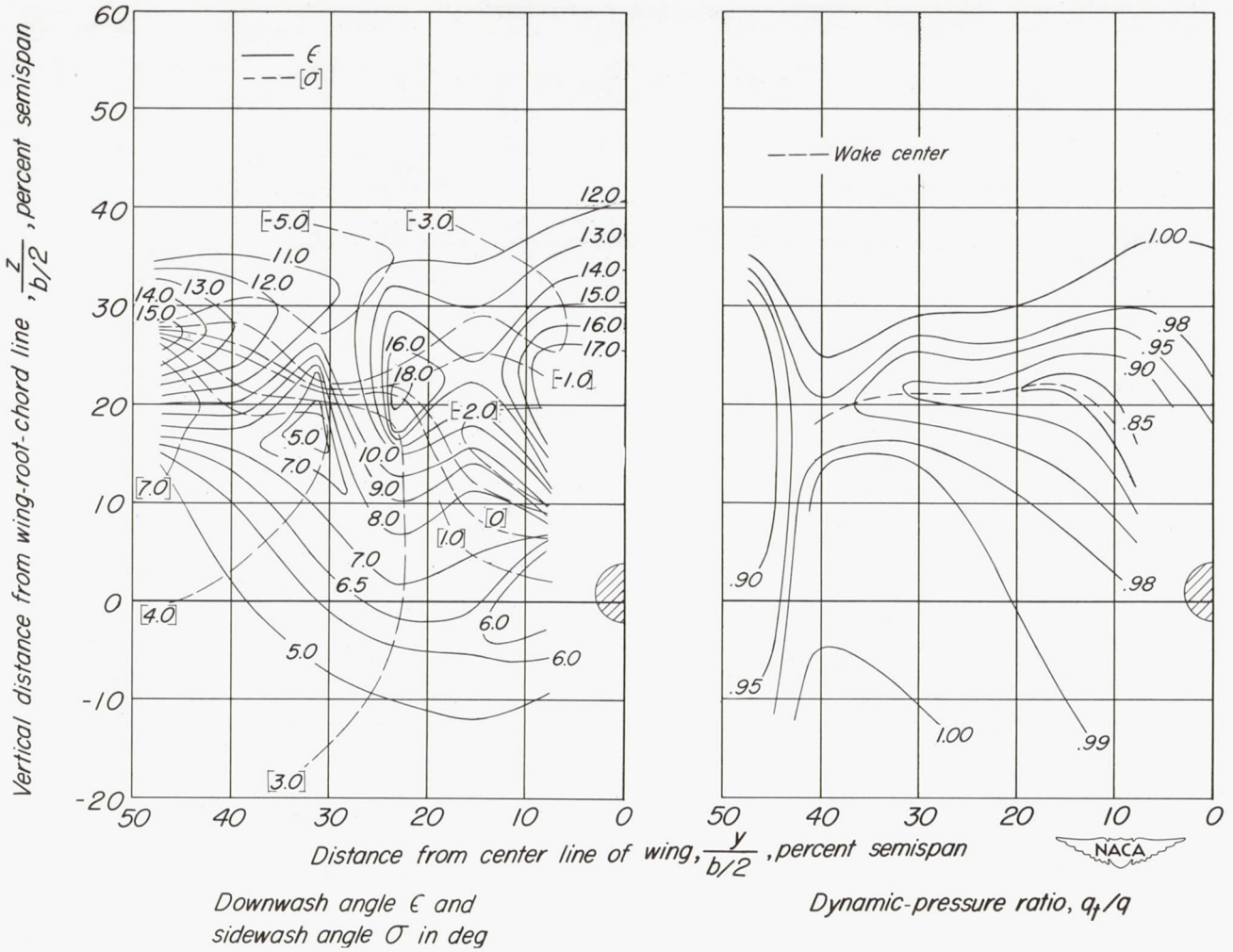
(b) $\alpha = 12.9^{\circ}$; $C_L = 0.83$.

Figure 8.- Continued.



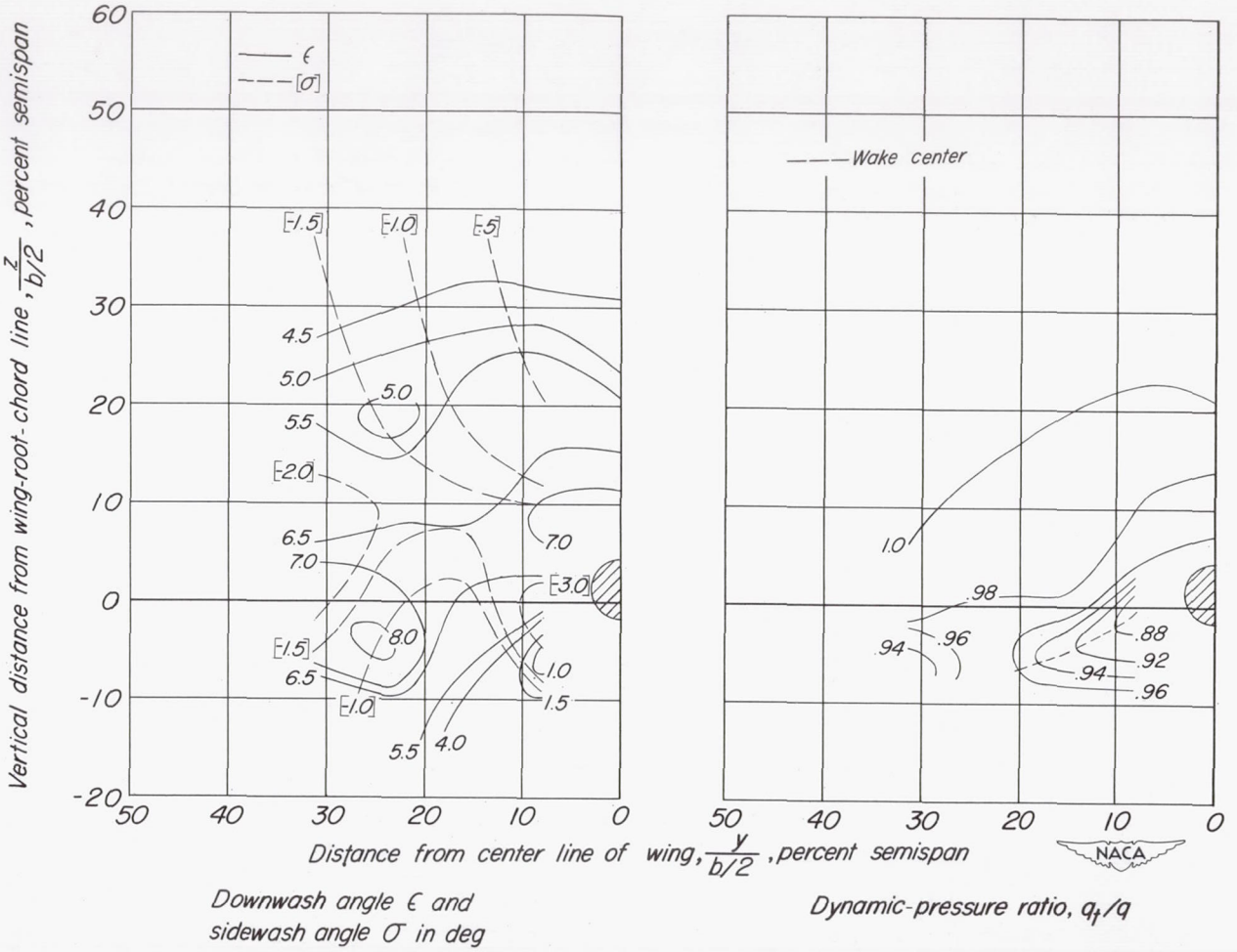
(c) $\alpha = 19.0^{\circ}$; $C_L = 1.04$.

Figure 8.- Continued.



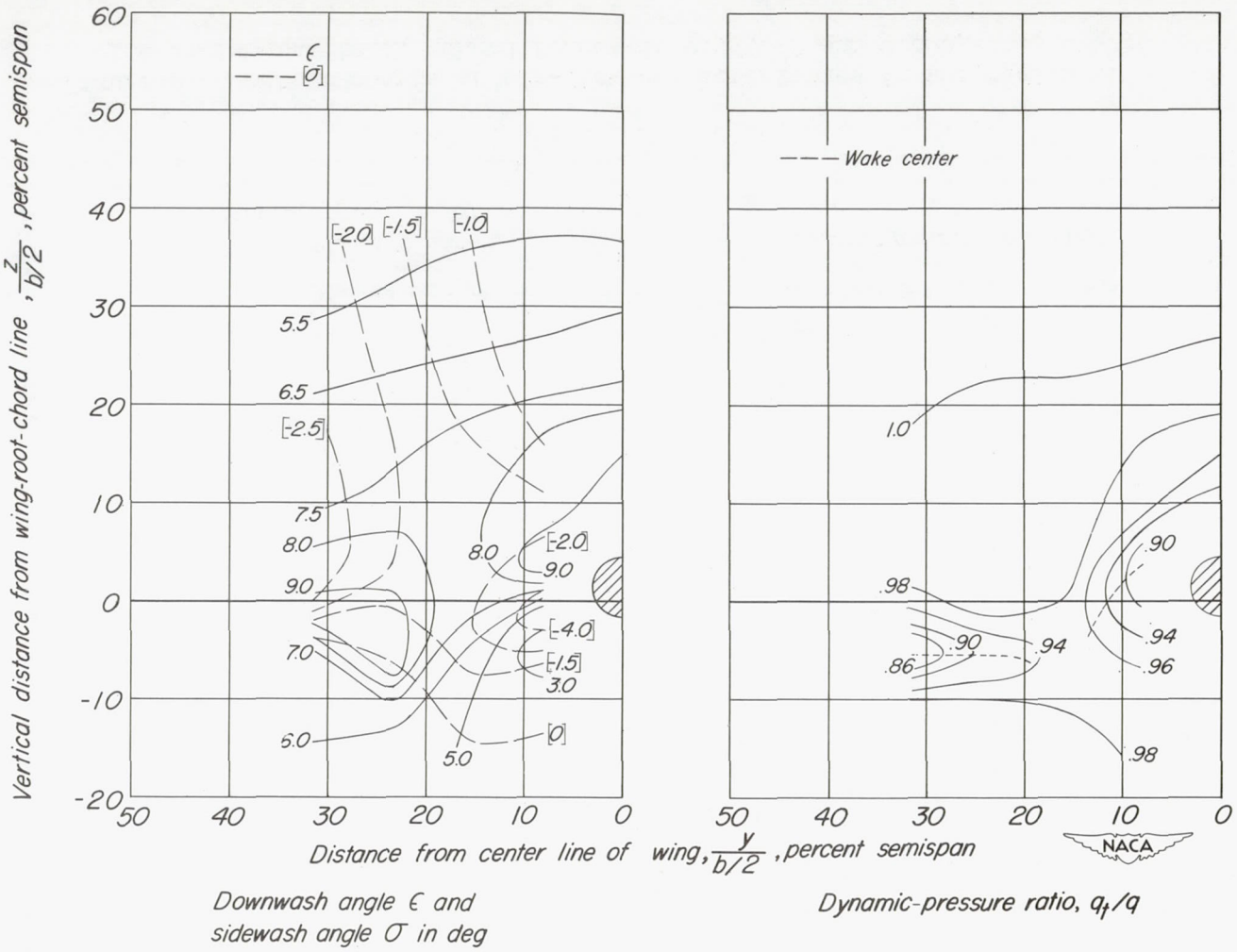
(d) $\alpha = 25.1^{\circ}$; $C_L = 1.25$.

Figure 8.- Concluded.



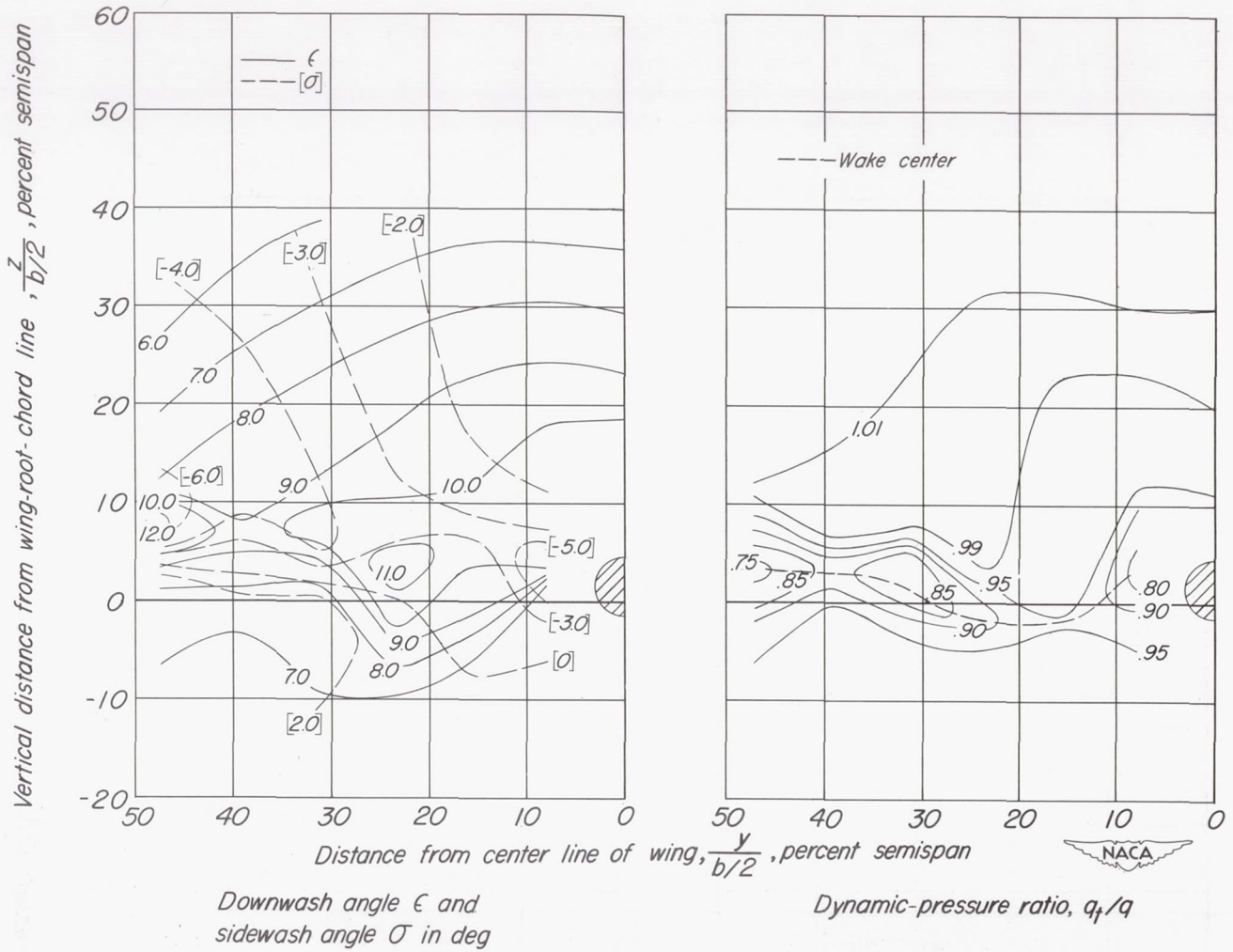
(a) $\alpha = 4.9^\circ$; $C_L = 0.66$.

Figure 9.- Contour charts of air-flow characteristics in the region of the horizontal tail. Chord fences at 0.575b/2 and 0.80b/2; $i_w = 4^\circ$; $\delta_f = 23^\circ$.



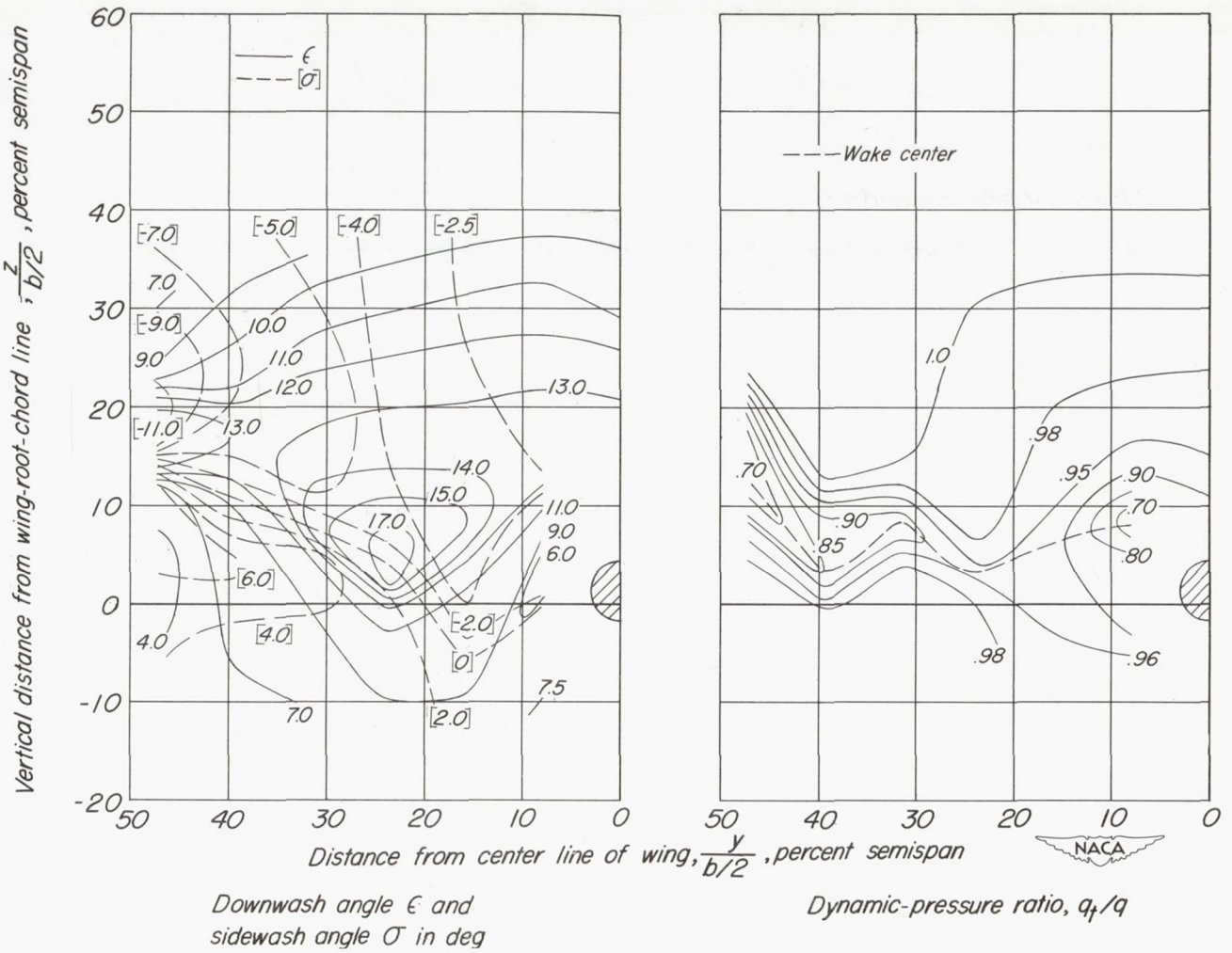
(b) $\alpha = 9.0^{\circ}$; $C_L = 0.96$.

Figure 9.- Continued.



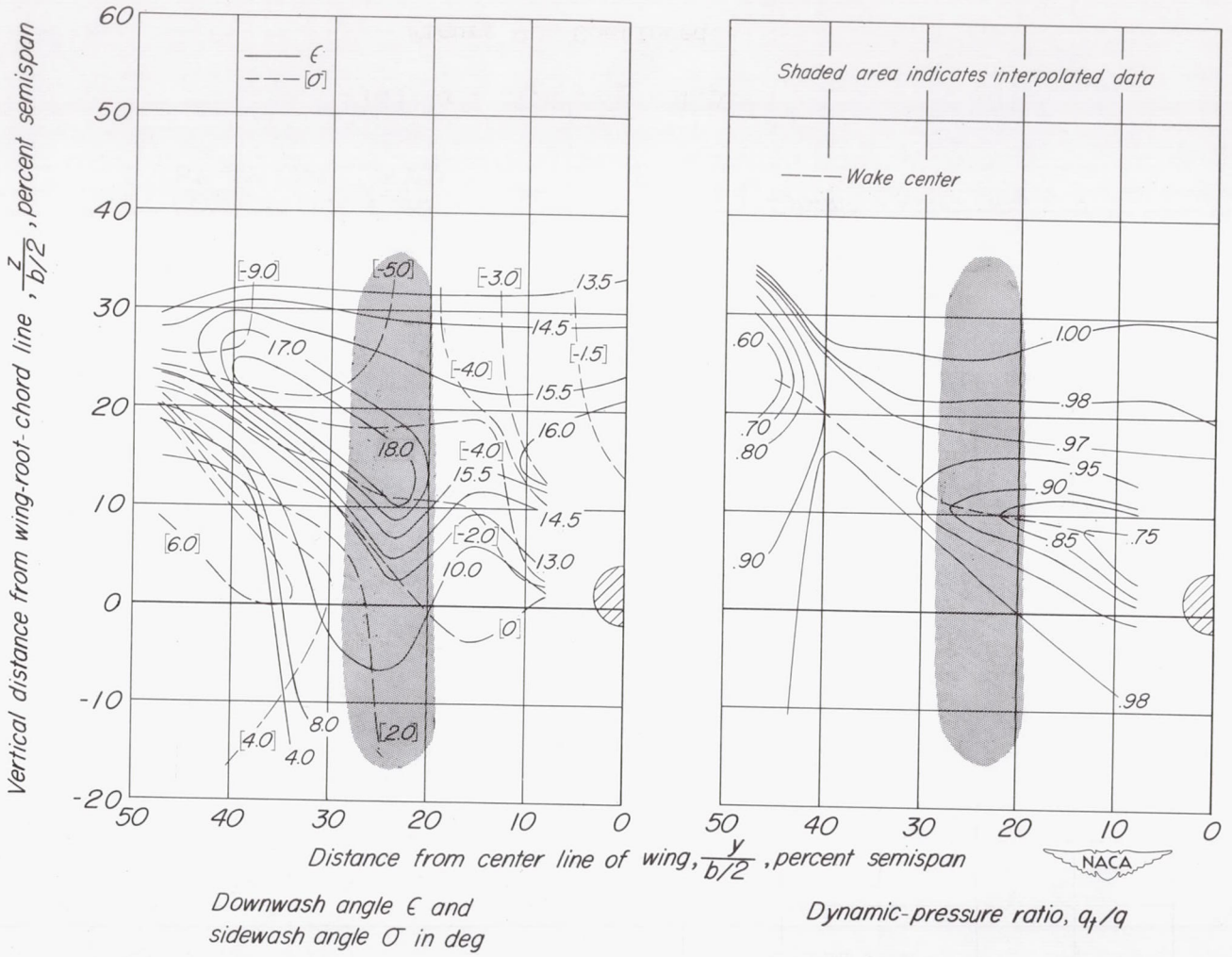
(c) $\alpha = 13.1^\circ$; $C_L = 1.19$.

Figure 9.- Continued.



(d) $\alpha = 19.2^{\circ}$; $C_L = 1.51$.

Figure 9.- Continued.



(e) $\alpha = 23.2^{\circ}$; $C_L = 1.64$.

Figure 9.- Concluded.